

AN EXTENDED AND MORE SENSITIVE SEARCH FOR PERIODICITIES IN RXTE/ASM X-RAY LIGHT CURVES

ALAN M. LEVINE¹, HALE V. BRADT^{1,2}, DEEPTO CHAKRABARTY^{1,2}, ROBIN H. D. CORBET³, AND ROBERT J. HARRIS⁴
Draft version October 30, 2018

ABSTRACT

We present the results of a systematic search in ~ 14 years of *Rossi X-ray Timing Explorer* All-Sky Monitor data for evidence of periodicities not reported by Wen et al. (2006). Two variations of the commonly used Fourier analysis search method have been employed to achieve significant improvements in sensitivity. The use of these methods and the accumulation of additional data have resulted in the detection of the signatures of the orbital periods of eight low-mass X-ray binary systems and of ten high-mass X-ray binaries not listed in the tables of Wen et al.

Subject headings: binaries: general — X-rays: stars

1. INTRODUCTION

We have extended the search of Wen et al. (2006) for periodicities in the intensities of X-ray sources using light curves produced by the *Rossi X-ray Timing Explorer* (RXTE) All-Sky Monitor (ASM). Wen et al. (2006) analyzed data accumulated during the first 8.5 years of the mission and detected 41 periodicities and 5 possible periodicities or quasiperiodicities. Two of the periodicities detected in their search likely represent neutron star spin and ~ 6 represent the precession of tilted accretion disks or other phenomena that produce superorbital periods. The 33 other periodicities are believed to represent evidence of the orbital motion of a close-binary star system. Most of the orbital periods were associated with high-mass X-ray binaries (HMXBs) where the normal type star is either a supergiant or a Be star. Eight of the periodicities were associated with the orbital periods of low-mass X-ray binaries (LMXBs), and one was associated with a cataclysmic variable (CV).

The search of Wen et al. (2006) was one of the most comprehensive searches for periodicities in the range of hours to years in the X-ray intensities of the bright Galactic X-ray sources. However, relatively few new periods were found in the course of the search in spite of the conventional wisdom that nearly all of the bright Galactic sources are accreting binaries with periods in the range of sensitivity of the search. The orbital periods of many Galactic sources are still not determined, and so searches for evidence of these presently unknown orbital periods remain of interest.

The present search improves on the sensitivity achieved in the earlier search through the analysis of light curves obtained over a longer course of time, i.e. nearly 14 years as opposed to 8.5 years, and through two major changes in the analysis techniques. We have also analyzed subintervals of the mission-long data sets. A pre-

liminary report of the results of this work was presented in Levine & Corbet (2006).

2. DATA

The ASM consists of three Scanning Shadow Cameras (SSCs) mounted on a rotating Drive Assembly (Levine et al. 1996). Each SSC acts as a coded-aperture camera and comprises a position-sensitive proportional counter (PSPC) that detects X-ray photons and provides one-dimension position information via the charge-division technique. The entrance window of each PSPC has a total geometric area of about 68 cm². A mask that is perforated with a pseudorandom pattern of open slits is held 30 cm above the PSPC entrance window. The mask open fraction is close to 50%. The field of view of each SSC is $6^\circ \times 90^\circ$ (FWHM). The ASM observations have almost entirely been made as series of 90-s exposures known as dwells. In each dwell the aspect of the assembly of SSCs is held fixed. For each exposure, a coded-aperture analysis of the data from each SSC yields intensity estimates of the sources that are listed in a catalog (hereafter the ASM catalog) and that fall within that SSC's field of view. The intensity estimates are derived for each of four spectral bands which nominally correspond to photon energy ranges of 1.5-3, 3-5, 5-12, and 1.5-12 keV and typically achieve a sensitivity of a few SSC counts s⁻¹ (the Crab Nebula produces intensities of 27, 23, 25, and 75 SSC counts s⁻¹ in the 4 bands, respectively). Any given source has been viewed in a large number, e.g., 30,000 to 100,000, of the 90-s exposures over the ~ 14 years of operation of the ASM. Each exposure generally yields intensity estimates for the four spectral bands.

The present search has been carried out, except where otherwise noted, using the ASM data acquired from the beginning of operations in early 1996 through 2010 January 28 (MJD 55224; Modified Julian Date = Julian Date - 2,400,000.5).

The coded-aperture analysis is applied to all ASM observations. The results are sorted source-by-source, filtered, and used to construct light curve files for each of 571 potential sources for each of the four energy bands. The intensity measurements contained in these files are the input data for the present periodicity search.

The instrument properties have changed over the 14

¹Kavli Institute for Astrophysics and Space Research, MIT, Cambridge, MA 02139, USA; aml@space.mit.edu, hale@space.mit.edu, deepto@mit.edu

²Physics Department, MIT, Cambridge, MA 02139, USA

³University of Maryland, Baltimore County, and X-ray Astrophysics Laboratory, Code 662, NASA/Goddard Space Flight Center, Greenbelt, MD 20771, USA; robin.corbet@nasa.gov

⁴Harvard-Smithsonian Center for Astrophysics, 60 Garden St., Cambridge, MA 02138, USA; rjharris@cfa.harvard.edu

years of operation in orbit because of at least three effects. First, the gain of SSC 1 (of SSCs 1-3) increased at about 10% per year for the first 13 years or so because of a leak in the counter entrance window (the rate of increase appears to have moderated in year 14). This has resulted, first, in progressive reductions in the effective sensitivity of SSC 1 in the 5-12 keV band and, recently, to some extent in the 3-5 keV band because in the last few years the pulse heights of higher energy events are often saturated and thus unusable.

The second of the effects is present because the one-dimensional position-sensing capability of the proportional counters is based on the charge-division technique and the resistivity of carbon-coated quartz-fiber anodes. The process of event detection in the counters results in the redistribution or removal of the carbon. The resistivity of each anode thus evolves over time generally becoming larger and less uniform, and so the functions that relate charge ratio to position have changed over the course of the mission.

Third, in the last few years there is often a high background of events that have pulse heights that suggest that they are due to the detection of Al $K\alpha$ photons. We do not understand in detail why this is happening but we speculate that it may be due to leakage of ultraviolet radiation through the Al-coated Kapton thermal shields that are immediately above the coded mask plates. UV radiation would produce photoelectrons at the counter body surfaces that happen to be, by design of the instrument, at potentials of approximately -1.8 kV. The photoelectrons would be accelerated toward and would hit, e.g., the aluminum collimators that are near the ground potential. Some fraction of the Al $K\alpha$ photons that would be produced by this process would then be detected.

Both the gain changes and charge ratio to position calibration changes are accounted for in detail in the detector model used in our coded-aperture analysis. However, the calibrations are imperfect and the derived source intensities are therefore somewhat affected by systematic errors on both short and long time scales. The coded aperture analysis is also designed to eliminate the effects of backgrounds that are smooth and slowly-varying with regard to position in the detector; this is largely but not entirely effective.

3. ANALYSIS

Searches for periodicities where large numbers of measurements are involved have generally proceeded by averaging the measured intensities in equally-spaced time bins, Fourier transforming the resulting time series, producing a power density spectrum by taking the absolute square of the complex amplitude for each frequency, and searching for peaks in the power spectrum. Our search largely follows this outline but we have implemented a few significant modifications as described below. In some searches for periodicities, a Lomb-Scargle periodogram (Scargle 1982; see also Press et al. 1992) is used in place of a Fourier transform, but, when large numbers of measurements and time bins are being analyzed, the differences between the two are not important except at extremely low frequencies. For the present analyses, the conventional discrete Fourier transform is adequate so we do not make use of the Lomb-Scargle variation.

We employ two unusual strategies with the goal of improving the search sensitivity. The first strategy involves the use of weights such as the reciprocals of the variances in Fourier and other types of analysis since the individual ASM measurements have a wide range of associated uncertainties. Since in the present instance the amplitudes in the Fourier transforms may be regarded as statistical averages, they may be better determined by the use of appropriate weights. This is discussed briefly in Corbet et al. (2007a) and at greater length in Corbet et al. (2007b). These two reports also discuss the use of weights which involve the intrinsic source variability, but we do not use such weights in the work reported herein.

The second strategy stems from the fact that the observations of the source are obtained with a low duty cycle, i.e., the window function is sparse but nevertheless highly structured. The properties of the window function, in combination with the presence of slow variations of the source intensity, act to hinder the detection of variations on short time scales. The window function power density spectrum (PDS) has substantial power at high frequencies, e.g., 1 cycle d^{-1} and 1 cycle per spacecraft orbit (~ 95 minute period). Since the data may be regarded as the product of a (hypothetical) continuous set of source intensity measurements with the window function, a Fourier transform of the data is equivalent to the convolution of a transform of a continuous set of intensity measurements with the window function transform. The high frequency structure in the window function transform acts to spread power at low frequencies in the source intensity to high frequencies in the calculated transform (or, equivalently, the PDS). This effectively raises the noise level at high frequencies. Thus, in most of our analyses, a smoothed version of the light curve is subtracted from the binned data prior to the Fourier analysis.

The details of the analysis of each ASM dwell-by-dwell light curve are as follows. The time of each intensity measurement was adjusted to approximately remove the effects of the motion of the Earth around the Solar System barycenter and the adjusted times were used to assign the measurements to equally-spaced time bins of duration 5 minutes (0.0034722 d) or more. Weights are used in averaging those measurements that fall into a given time bin. The n_i measurements that fall into the time bin which is labelled by the index i are denoted with index j that runs from 1 to n_i . We denote the j th measured source intensity in a time bin by s_j and its associated 1-sigma uncertainty by σ_j . The averaging in this stage uses weights $w_j = 1/\sigma_j^{k_A}$ where k_A is a selected weighting index (see values in Table 1). The weighted-average intensity in bin i is then

$$d_i = \frac{\sum_{j=1}^{n_i} s_j / \sigma_j^{k_A}}{\sum_{j=1}^{n_i} 1 / \sigma_j^{k_A}} \quad (1)$$

For convenience we denote the denominator of this expression by W_i so that

$$W_i = \sum_{j=1}^{n_i} 1 / \sigma_j^{k_A}. \quad (2)$$

TABLE 1
ANALYSIS METHOD VARIATIONS

Method Name	Smoothing Kernel	Weight Index k_A	Weight Index k_B
unwt	none ^a	2.0	0.0
wt	none ^a	2.0	2.0
ungs	Gaussian	2.0	0.0
wtgs	Gaussian	2.0	2.0
wtgs-v4	Gaussian	2.5	1.5
wtgs-v8	Gaussian	2.0	3.0
wtbx	box	2.0	2.0

^a No subtraction of a smoothed version of the light curve was done in this case.

where it should be understood that $W_i = 0$ for those time bins that contain no measurements. The W_i 's are used to weight the time bins in the subsequent analysis.

As stated above, a smoothed version of the light curve is, in many of our analyses, subtracted from the binned data. The smoothed version is given by a time bin by time bin ratio in which the numerator is computed by convolving a kernel function with a weighted version of the binned light curve. The denominator is computed by convolving the same kernel function with a weighted version of the window function. The value of the i th bin of the smoothed data is given by

$$D_i = \frac{(K \otimes (W \cdot d))_i}{(K \otimes W)_i} \quad (3)$$

where K represents the kernel function, d and W are the above defined functions of the time bin index i , and " \otimes " denotes convolution. The kernel function K may be either a Gaussian or a box function. In the case of the Gaussian kernel, the full width at half maximum response is taken to be equal to the smoothing time parameter. The Gaussian is calculated out to ± 14 standard deviations from its center. In the case of the box function, the box width is taken to be twice the smoothing time parameter. The convolution is accomplished using Fourier transforms.

We repeated the analyses using seven different values of the smoothing time parameter (see Table 2) to optimize the sensitivity in each of several different frequency ranges. In each case the smoothed light curve was subtracted from the unsmoothed light curve, weights were applied, and the results were Fourier transformed. In symbols, this part of the analysis produces a filtered light curve described by:

$$F_i = Y_i(d_i - D_i) \quad (4)$$

where the weights Y_i are given by

$$Y_i = W_i^{k_B/k_A} = \left[\sum_{j=1}^{n_i} 1/\sigma_j^{k_A} \right]^{k_B/k_A} \quad (5)$$

and k_B is a second weighting index. Weight index values are given in Table 1. We also did the analysis without subtracting a smoothed version of the light curve.

The unweighted average of the set of F_i 's which correspond to bins with nonzero exposure is computed and then subtracted from each of the F_i values for those bins. The resultant array is extended with zeroes by a factor of four and Fourier transformed. The extension of the

array yields oversampling in the frequency domain. The oversampled transform is converted into a power density spectrum which is normalized to have an average value of unity.

The normalized power spectra are compressed by saving the average and maximum values for sets of contiguous frequency bins; the number of contiguous bins depends on the frequency range and smoothing time parameter (see Table 2).

We found that for the analyses where short smoothing time scales were used, i.e., time scales of 0.3, 0.9, and 3.0 days, the compressed power spectra have a non-white appearance. The effect is strongest for the shortest smoothing time scale, i.e., 0.3 days. It is not clear how to apply a threshold for detection of a periodicity in a nonwhite spectrum. Therefore we added a procedure (to the code that performs the compression described above) to compute a "background" average power around each compressed frequency bin, and to then obtain whitened maximum values. Each whitened maximum value is then the ratio of a maximum value in an unwhitened compressed spectrum to the corresponding background average. The resulting whitened spectra generally appear to have little systematic structure (see Fig. 1).

Table 1 lists, at the highest level, the variations of the analysis method that we have used. We found that the results from the methods where both weighting and filtering were applied ("wtgs", "wtgs-v4", "wtgs-v8", and "wtbx") were almost always nearly equal or superior to the results obtained with the other methods ("unwt", "wt", "ungs"). A typical, i.e., not the extreme best case, of the differences is illustrated in Figure 2. Therefore we did not search for significant peaks in the power spectra obtained using the latter methods. The "wtgs", "wtgs-v4", "wtgs-v8", and "wtbx" methods were all applied to the 1.5-12 keV band light curves, but the results generally produced power spectra that were quite similar in terms of both detailed appearance and sensitivity. Therefore only the "wtgs" method was applied to the other three energy bands. The results from the four energy bands are, in some cases, quite different from each other. Table 2 lists smoothing time scales and the corresponding bin durations, parameters used for compression and whitening, and parameters used in searching for significant peaks.

The powers in a spectrum of Gaussian white noise are expected to be well characterized by an exponential probability distribution. We make the assumption that the powers in the whitened spectra computed as described above similarly follow an exponential distribution. In the present case it is not clear how to precisely compute the number of independent bins that we examined because 1) some of the power spectra for a given source involve the same data and differ only on account of slight variations in the analysis procedure, and 2) there is a significant degree of dependence among the powers in an oversampled power spectrum. Although it is not fully justified on an a priori basis, we simply estimate the number of independent bins N_{ind} by the product of the number of frequency bins that would have applied if the Fourier spectrum had not been oversampled, the number of energy bands analyzed (4; this neglects the non-independent bins among the four slightly different analyses of the 1.5-12 keV band), and the number of

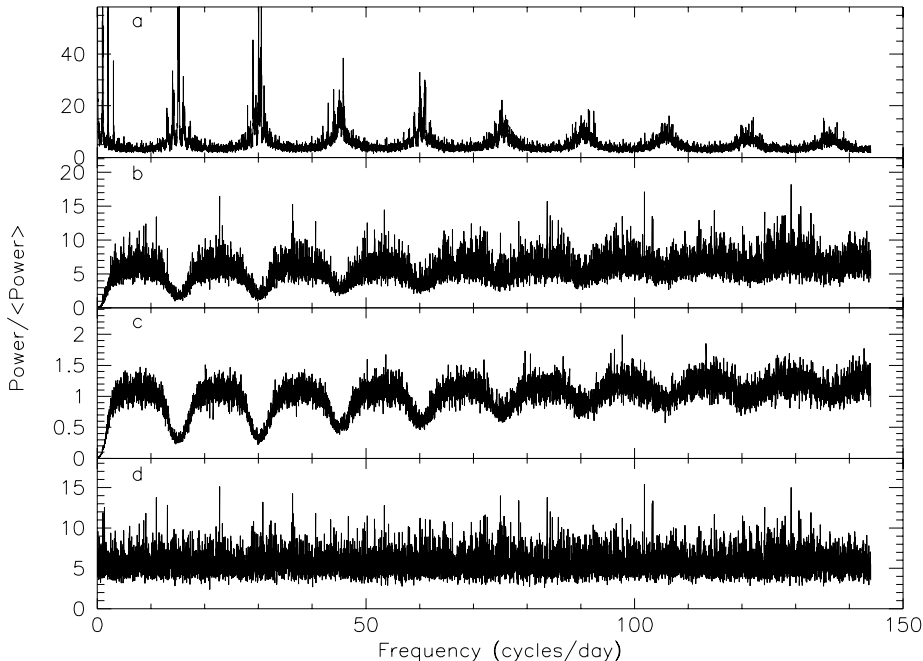


FIG. 1.— Power density spectra (PDSs) based on the 1.5–12 keV ASM light curve of LMC X-2. These PDSs were made using a smoothing time scale of 0.3 days and have been compressed using the standard parameters (Table 2); they illustrate the compression and whitening procedure used in the search (see text). The Nyquist frequency is 144 d^{-1} . a) PDS of the window function, i.e., of the weights used in the analysis of the data. For this example the weights are the reciprocals of the formally-estimated variances of the binned data. Those time bins of the window function which do not contain any measurements are assigned weights of zero. Prominent peaks are seen at frequencies of 1 d^{-1} and $\sim 15 \text{ d}^{-1}$, i.e., the orbital frequency of the *RXTE* spacecraft, and harmonics thereof. Some of the strong peaks extend substantially above the upper boundary of the plot. b) The maximum values of each set of 300 contiguous bins of the light curve PDS. c) The average values of each set of 300 contiguous bins of the light curve PDS. d) The whitened maximum values of the PDS consisting of the maximum values shown in (b) divided by a local (in frequency) background determined from (c). In this example, no power is seen that exceeds the detection threshold.

TABLE 2
FILTERING TIMESCALES AND PARAMETERS

Time Scale (days)	Bin Time (days)	N_{rebin}	N_{avg}	N_{some}	ν_{low} (d^{-1})	ν_{hi} (d^{-1})	Threshold Power
none	2.0	1	300	3	0.0007	1.0	17.7
500.0	2.0	1	300	3	0.004	1.0	17.7
100.0	1.0	1	300	3	0.022	1.0	18.4
30.0	0.15	10	60	1	0.1	4.0	20.3
10.0	0.05	20	30	1	0.2	10.0	21.4
3.0	0.005	150	12	1	0.66	100.0	23.7
0.9	0.0034722222	300	6	1	2.2	144.0	24.1
0.3	0.0034722222	300	6	1	6.6	144.0	24.1

sources (571). The neglect of the oversampling factor and the multiple similar analyses of the sum band does not appear to have led to significant underestimates of the detection thresholds, and, thus, this procedure appears to be justified.

We have chosen a detection threshold P_{thr} for previously unknown periodicities to limit the expected number of false detections N_{exp} produced by statistical fluctuations (based on the assumption that the powers are exponentially distributed) in the power spectra calculated using a given smoothing time parameter. Thus we have

$$N_{\text{exp}} = N_{\text{ind}} e^{-P_{\text{thr}}} \quad (6)$$

so that

$$P_{\text{thr}} = \log N_{\text{ind}} - \log N_{\text{exp}}. \quad (7)$$

The values of P_{thr} are given in Table 2 for $N_{\text{exp}} = 0.1$.

As can be seen in Figs. 1 and 2, the window functions of the light curves often contain strong peaks at or close to particular frequencies. Even though the analysis procedure tends to minimize the appearance of these frequencies in the whitened power spectra, there are occurrences of peaks at these frequencies. In the analyses done with filtering based on smoothing time scales of 10.0 days and under, we ignore all peaks in the frequency ranges 1.00 ± 0.04 , 2.00 ± 0.04 , 15.15 ± 0.20 , 30.3 ± 0.2 , 45.45 ± 0.20 , and $60.6 \pm 0.2 \text{ d}^{-1}$. For the other analyses, we ignore all peaks in the frequency ranges 0.00274 ± 0.00025 , 0.00548 ± 0.00025 , 0.01096 ± 0.00025 , 0.01644 ± 0.00025 , 0.01900 ± 0.00035 , 0.01960 ± 0.00025 , 0.02450 ± 0.00025 , and $0.02500 \pm 0.00025 \text{ d}^{-1}$.

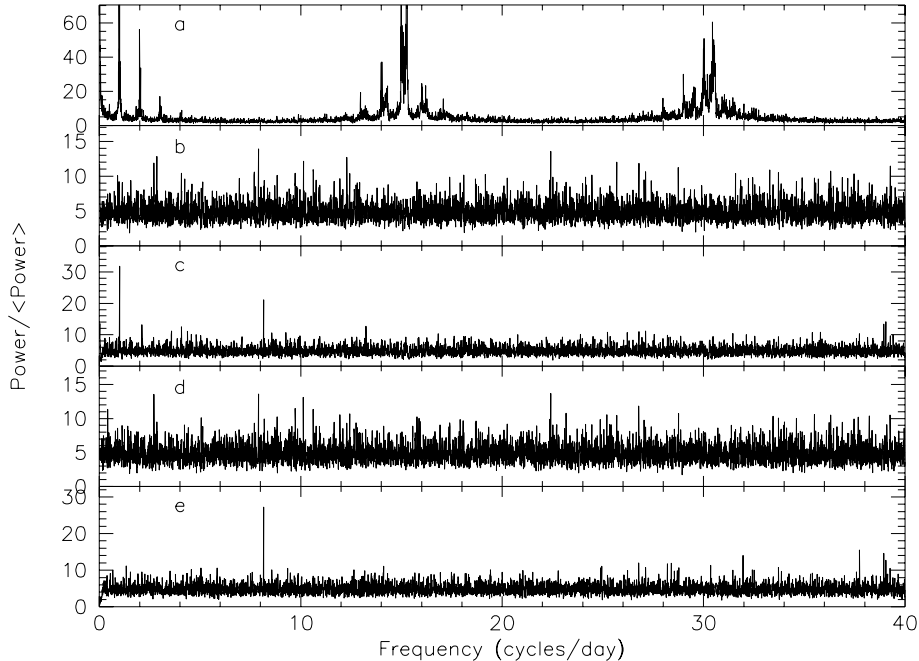


FIG. 2.— Power density spectra (PDSs) based on the 1.5–12 keV ASM light curve of X1323–619 that illustrate the typical differences in the results obtained over a representative set of variations of the analysis algorithm. The PDSs in panels b–e have been compressed using the standard parameters for the 3.0 day smoothing time scale (see Table 2); the whitened maximum powers are shown here. The Nyquist frequency is 100 d^{-1} , but only frequencies up to 40 d^{-1} are shown. a) PDS of the window function; see the caption for Fig. 1. b) PDS computed with intensities that are neither weighted nor filtered by subtraction of a smoothed version of the light curve (“unwt” entry in Table 1). c) PDS computed with intensities that are weighted but are not filtered (“wt” in Table 1). d) PDS computed with intensities that are not weighted but are filtered (“ungs” in Table 1). The light curve was smoothed using a 3.0 day time scale for use in the filtering for the PDSs shown in this panel and in panel e. e) PDS computed with intensities that are both weighted and filtered (“wtgs” in Table 1). A signal is apparent at the $\sim 8.15 \text{ d}^{-1}$ orbital period of X1323–619 (See Table 3) in panel c but is seen with an even higher amplitude in panel e. No peak stands out at this frequency in either panel b or d.

A substantial fraction of the 571 potential sources are extragalactic targets such as active galactic nuclei, extended Galactic targets such as supernova remnants, or X-ray binaries that have been in quiescence since the beginning of the RXTE mission and for which we have no expectation of finding detectable periodicities. The power spectra of these sources act effectively as controls that show the actual statistics of the power spectra and that bring attention to periodicities that must be the product of statistical fluctuations or artifacts. Indeed, the search procedure described here was tailored in part by examination of the results on the “controls”. Furthermore, since it would be difficult to understand the reality of peaks that exceed the detection threshold in the power spectra of these sources, the effective number of sources must be less than 571. We have not adjusted the significance thresholds downward to account for this effect.

Since we searched large numbers of bins, the thresholds for the detection of previously unreported periodicities given in Table 2 are high. When a periodicity has previously been reported, it may be confirmed even if the power at or very close to the previously reported frequency is below the threshold given in the table.

Uncompressed power density spectra are useful for precise estimation of the frequencies of the detected periodicities. Since the uncompressed spectra were not saved in the original analysis for smoothing time scales less than or equal to 30.0 days, the analyses that produced

the most significant detection of each periodicity were repeated, if necessary, and the resulting uncompressed spectra were saved. For each periodicity a small frequency range around the major peak was fit with a Gaussian to obtain estimates of the central frequency, its uncertainty, and the peak width. The uncertainty in the frequency may be estimated based on the result of Horne and Baliunas (1986) that

$$\delta f_1 = \frac{3}{8} \frac{1}{T\sqrt{P_r}} \quad (8)$$

where T is the length of the time interval covered by the light curve and P_r is the peak power in a normalized PDS. We also use the simple estimate

$$\delta f_2 = \frac{1}{2T} \quad (9)$$

which, in most cases, should be a conservative upper limit to the uncertainty (but, if the periodicity persisted for only a fraction of the time covered by the light curve, the uncertainty could be larger than this value). In the estimates of frequencies and periods that we present below, the uncertainty derived using eq. (8) is given first and the uncertainty derived using eq. (9) is given second in square brackets.

4. RESULTS

In the present search we find clear evidence of the periodicities in GRO J1008–57 and SS 433 that have been

previously detected in the ASM data but had not been detected in the analysis reported by Wen et al. (2006). Wen et al. (2006) reported the detection of the 9.56-day period of 4U 2206+543, but did not find evidence of variation with a period of ~ 19.1 days. Such variation was first reported by Corbet et al. (2007b). Since we now find clear evidence of variation at the ~ 19.1 -d period, we report its detection herein.

In the previous section, we noted that periodicities at previously identified frequencies can be found with better sensitivity than periodicities at undetermined frequencies. Therefore we examined the power spectra for peaks at the frequencies corresponding to the periods listed in the catalogs of Bodaghee et al. (2007) and Liu et al. (2006, 2007) and thereby identified evidence of the presence of a number of periodicities that were not found by Wen et al. (2006).

Table 3 lists the periodicities that emerge from the present search that are not listed in Tables 1-3 of Wen et al. (2006). Only one of these was, when first detected in the course of this search, previously unreported on the basis of optical or other X-ray observations, namely the 18.545-day periodicity in IGR J18483–0311. The photon energy band, filter time scale, and method that yielded the most significant detection are given for each detected periodicity. The estimated frequencies and associated uncertainties are listed in Table 3 with the exception of the very low frequencies of the sources GRO J1008–57 and 2S 1845–024. The frequencies or, equivalently, periods of these latter sources are better obtained from epoch-folding analyses and even more precisely from pulse timing studies.

We give in Table 4 average source intensities, peak powers seen in the whitened and renormalized power spectra, and estimated average amplitudes of the detected periodic signals. The source names, photon energy bands, and periods are taken from Table 3.

The estimated average amplitudes of the detected periodic signals were obtained by superposing sine waves onto the measured intensities in the appropriate light curves and redoing the complete analysis using the appropriate method, time scale, and energy band. The sine wave frequencies were chosen to yield peaks in the power spectrum close to, but not on top of, the frequencies of the detected signals. The sine wave amplitudes were chosen to give peak powers close to or above, within a factor of two, the peak powers of the detected signals. The results were then interpolated to estimate the amplitudes that would give rise to the peak powers of the detected signals. The uncertainty in the amplitude for a given source was estimated by the rms dispersion in the amplitudes obtained when sine waves were injected at four to ten different frequencies.

In the last column of Table 4 we give the ratio of the inferred average signal amplitude (A) to the weighted average source intensity (I). This is an indicator of the fractional variation of the source intensity at the orbital frequency. It does not include the effects of harmonics which are detected in some of the power density spectra and should, therefore, be used only as a general indicator of the degree of modulation.

The ASM light curves of the sources for which we report detections of periodicities in Table 3 were folded at periods close to, i.e., within a small fraction of the quoted

1σ errors, those listed in that table. Weights were used in averaging the intensities in each phase bin. A smoothed version of the light curve was subtracted from each light curve before it was folded. The time scales used for the smoothing are listed in Table 3. After the folding was accomplished, the overall average intensity was then added to the folded light curve to show the proper mean (the mean was removed when the smoothed version was subtracted from the light curve). The folded light curves are shown in Figures 3 and 4.

The uncertainties shown in the plots of the folded light curves were determined from propagation of the 1σ uncertainties associated with each measurement in a light curve assuming the measurements are statistically independent. This neglects the effects of random source variability in at least two respects. First, the effects of source variability are not included in the formal uncertainties of the individual measurements. Second, when variability is present it almost always involves correlations from measurement to measurement.

The epochs of phase zero used in plotting the folded light curves are listed in Table 3. These epochs were determined by fitting each folded 1.5-12 keV band light curve with a combination of constant, sine, and cosine functions of phase. The epoch is then obtained from the phase of minimum or maximum intensity of the fitted function. Actual minima or maxima may deviate somewhat from these epochs; the differences may be seen in the folded light curves.

4.1. Additional Detections of Low-Mass X-ray Binaries

In this section we briefly discuss our results for each of the periodicities of the LMXBs listed in Table 3. The results in Table 3 show that, with only one exception, the most significant detections of these systems were made in the overall 1.5-12 keV energy band.

2S 0921–630 is a weak X-ray source in a low-mass system with a relatively long orbital period. Photometry of the bright optical counterpart by Chevalier & Ilovaisky (1981) and Branduardi-Raymont et al. (1981) suggested that the observed variability could be periodic, but did not yield correct estimates of the actual period. X-ray observations with the *EXOSAT* satellite showed intensity changes, interpreted as partial eclipses, that were key to obtaining the first relatively precise period estimate (Mason et al. 1987). Recent optical observations have also yielded relatively precise estimates of the orbital period; Shahbaz et al. (2004) obtained $P = 9.0035 \pm 0.0029$ d and Jonker et al. (2005) obtained $P = 9.006 \pm 0.007$ d. The orbital period is detected in the present study; this is shown in the power spectrum plotted in Fig. 5. We derive an estimate of the orbital period of $P = 9.009 \pm 0.001$ [± 0.008] d (see Table 3) that is consistent with these recently reported values. Shahbaz & Watson (2007) and Steeghs & Jonker (2007) report further work on the binary parameters including the component masses. The folded ASM light curves show that the periodic modulation has an amplitude of $\sim 30\%$ relative to the average source strength. However, the average source intensity could be affected by systematic errors in the baseline level of order 0.1 SSC counts s^{-1} (1.5-12 keV band). Nonetheless, the modulation fraction must be rather large, and the periodicity may

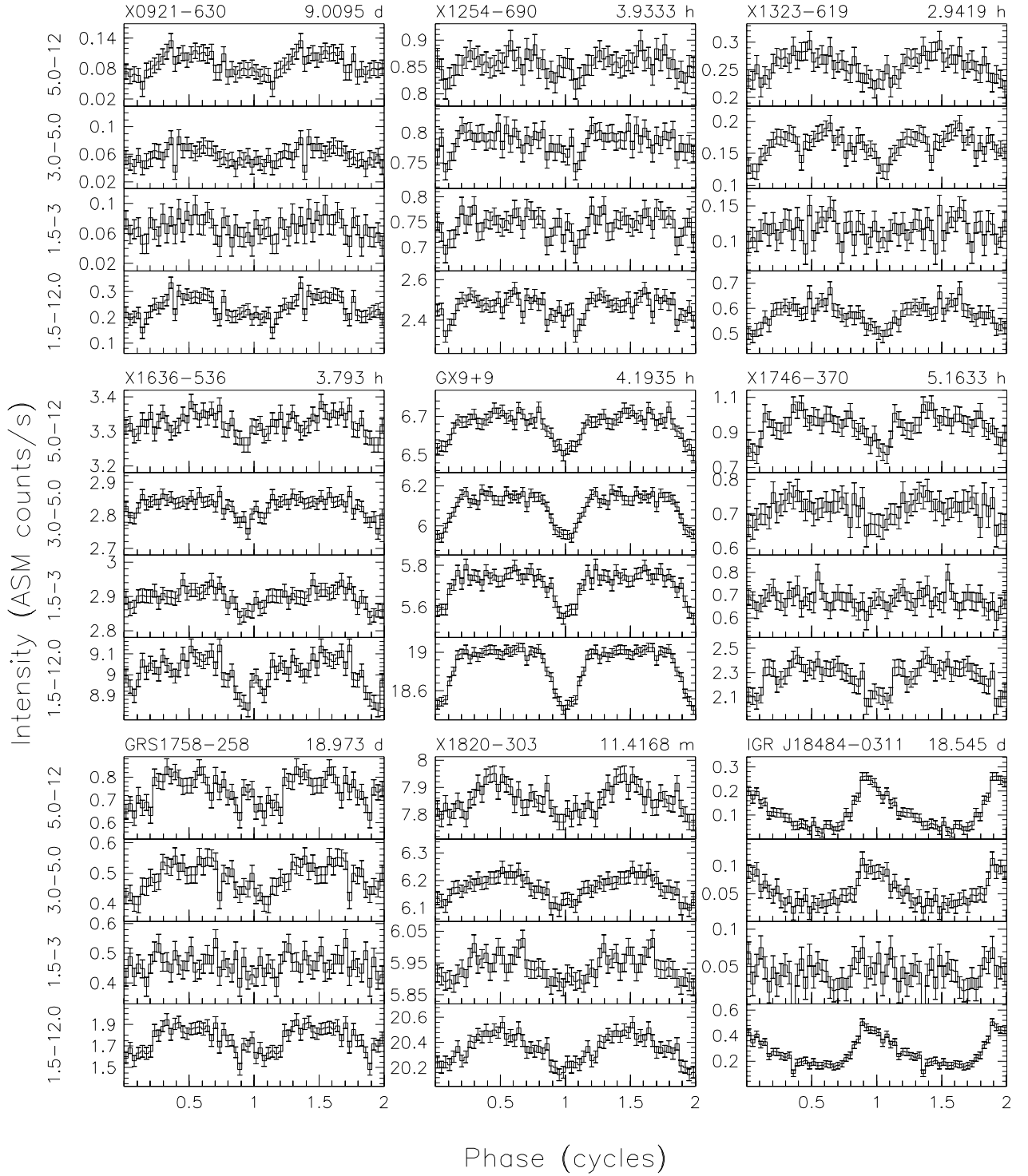


FIG. 3.— ASM light curves of 9 sources folded at the orbital periods given in Table 3. See the text for information on the details of the folding algorithm and the error bars shown here. For each source the folded light curves are shown for two full cycles for each of four energy bands.

TABLE 3
ADDITIONAL PERIODICITY DETECTIONS

Source Name ^a	ASM Catalog Entry	Band (keV)	Filter Time ^b (days)	Method ^c	Frequency ^d (cycles d ⁻¹)	Period ^d	Epoch ^e (MJD)
LMXB orbital periods							
2S 0921–630	x0921–630	1.5-12	30.0	wtbx	0.110994 (13; 100)	216.23 (3; 19) h	52738.13 (13)
4U 1254–69	x1254–690	1.5-12	3.0	wtgs-v4	6.101690 (15; 100)	3.933337 (10; 64) h	52733.0546 (31)
4U 1323–62	x1323–619	1.5-12	3.0	wtgs	8.157930 (15; 100)	2.941923 (5; 36) h	52733.2395 (18)
4U 1636–536	x1636–536	1.5-12	0.9	wtgs	6.327232 (14; 100)	3.793128 (8; 60) h	52733.0343 (18)
4U 1728–16 ^j	gx9+9	1.5-12	0.9	wtgs	5.723207 (7; 100)	4.193453 (5; 73) h	52733.152 (1)
4U 1746–37	x1746–370	1.5-12	3.0	wtgs-v8	4.648202 (15; 100)	5.163287 (18; 111) h	52733.156 (3)
GRS 1758–258	grs1758–258	3-5	500.0	wtgs	0.052706 (19;100)	18.973 (7; 36) d	52748.27 (23)
4U 1820–30	x1820–303	1.5-12	0.9	wtgs	126.129380 (13; 100)	0.19028081 (2; 15) h	52733.00590 (7)
HMXB orbital periods							
A 0535+26	x0535+26	1.5-12	500.0	wtgs	0.00906 ^f	110.4 ^f	52852.59 (27)
LMC X-1	lmcx1	1.5-12	100.0	wtbx	0.255821 (14; 100)	3.90898 (21; 153) d	52733.952 (45)
GRO J1008–57	groj1008–57	3-5	500.0	wtgs		^g	
2S 1417–62	x1417–624	5-12	100.0	wtgs	0.023611 (45; 100)	42.35 (8; 18) d	52770.04 (91)
IGR J16320–4751	igrj16320–4751	5-12	100.0	wtgs	0.111234 (11; 100)	8.9901 (9; 81) d	52742.79 (12)
IGR J16418–4532	igrj16418–4532	5-12	30.0	wtgs	0.267461 (20; 100)	3.73886 (28; 140) d	52735.84 (7)
EXO 1722–363	exo1722–363	5-12	30.0	wtgs	0.102655 (19; 100)	9.7414 (18; 95) d	52738.25 (19)
IGR J18027–2016	igrj18027–2017	5-12	30.0	wtgs	0.218881 (16;100)	4.5687 (3;21)	52736.36 (42)
2S 1845–024	x1845–024	5-12	500.0	wtgs		^h	
IGR J18483–0311	igrj18483–0311	5-12	100.0	wtgs	0.053923 (9; 100)	18.545 (3; 34) d	52754.37 (10)
3A 1909+048 ^k	ss433	5-12	100.0	wtgs	0.076452 (20; 100)	13.080 (3; 17) d	52745.19 (18)
4U 2206+543	x2206+543	1.5-12	100.0	wtbx	0.104620 (13; 100) ⁱ	9.5584 (12; 91) ⁱ d	52740.97 (6)

^a The source name is generally that listed first by Liu et al. (2007) or Liu et al. (2006).

^b See text and column 1 of Table 2.

^c See text and Table 1.

^d Estimated from the peak centroid. The uncertainties are shown in parentheses in units of the least significant digit and were obtained from eqs. (8) and (9).

^e Epoch of X-ray minimum or maximum (see phase zero in each light curve shown in Figs. 3 and 4).

^f The ASM power spectrum indicates the periodicity is present but is not useful for precisely estimating the orbital frequency and period. The values given are the best estimate from the ASM spectrum. The orbital period is estimated to be 110.3 ± 0.3 days via pulse timing (see text). The corresponding frequency is 0.009066 ± 0.000025 d⁻¹.

^g A peak power of 12 is seen in the second harmonic (first overtone). See Fig. 14.

^h A peak power of 11 is seen in the second harmonic (first overtone). See Fig. 14.

ⁱ The frequency and period given are those estimated from the strongest peak in the power spectrum.

^j 4U 1728–16 = GX 9+9

^k 3A 1909+048 = SS 433

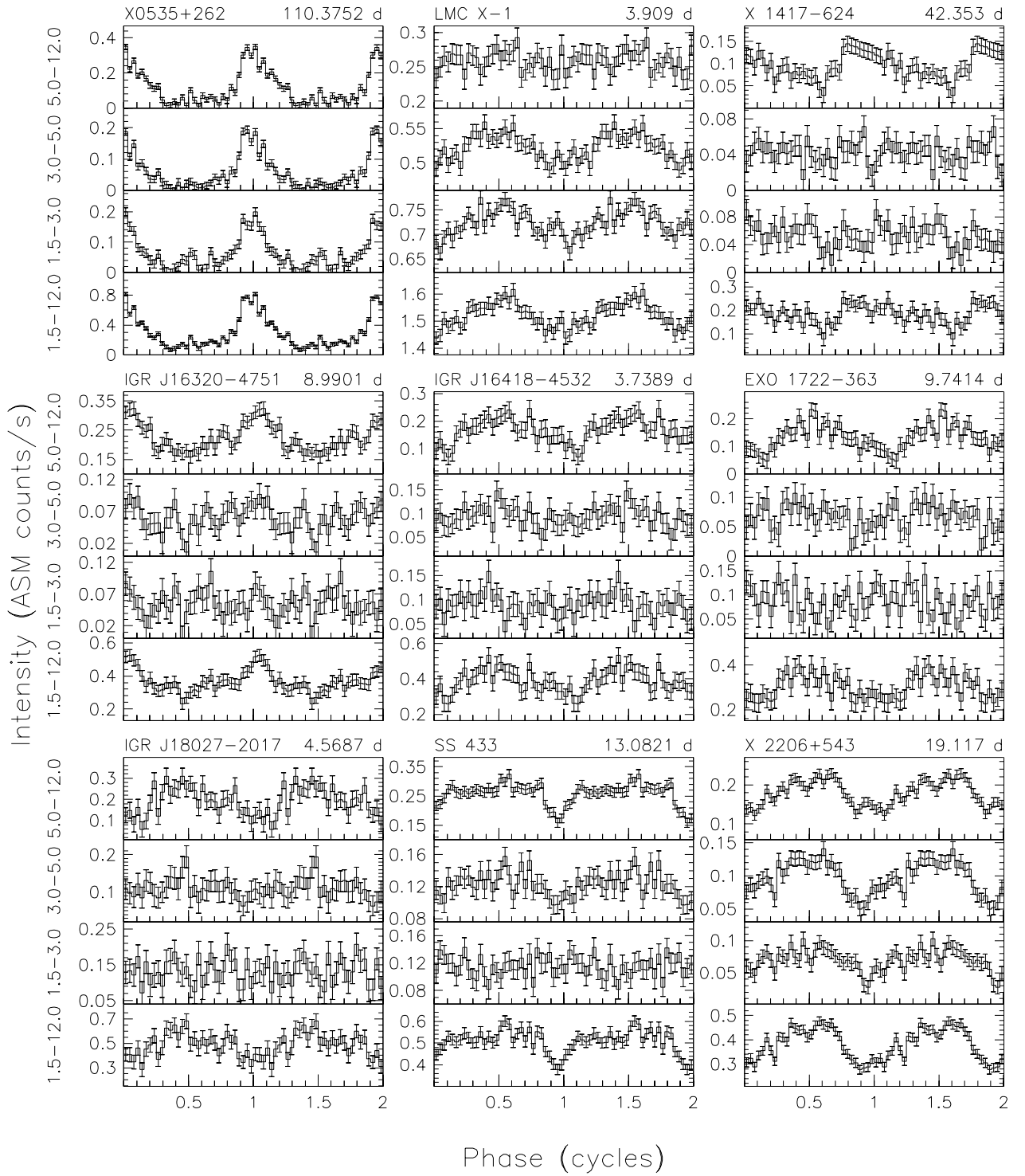


FIG. 4.— ASM light curves of 9 sources folded at the orbital periods given in Table 3.

TABLE 4
CHARACTERISTICS OF DETECTED PERIODICITIES

Source Name	Band (keV)	Wtd. Avg. Intensity ^a (cts s ⁻¹)	Unwtd. Avg. Intensity ^b (cts s ⁻¹)	Approx. Period	Power ^c	Amplitude ^d (cts s ⁻¹)	A/I ^e
LMXB orbital periods							
2S 0921–630	1.5-12	0.239 (4)	0.084 (6)	216.2 h	23	0.052	0.22
4U 1254–69	1.5-12	2.455 (4)	2.291 (6)	3.933 h	22	0.052	0.021
4U 1323–62	1.5-12	0.575 (4)	0.449 (6)	2.942 h	27	0.055	0.096
4U 1636–536	1.5-12	9.069 (6)	9.339 (9)	3.793 h	22	0.087	0.0096
4U 1728–16 (GX 9+9)	1.5-12	18.879 (8)	19.01 (1)	4.193 h	123	0.283	0.015
4U 1746–37	1.5-12	2.275 (6)	2.06 (1)	5.163 h	30	0.094	0.041
GRS 1758–258	3-5	0.485 (5)	0.391 (7)	18.97 d	13	0.054	0.11
4U 1820–30	1.5-12	20.347 (8)	20.63 (1)	0.1903 h	30	0.12	0.0059
HMXB orbital periods							
A 0535+26	1.5-12	0.275 (4)	0.550 (6)	110.4 ^f	11	0.21	0.78
LMC X-1	1.5-12	1.524 (4)	1.369 (5)	3.909 d	29	0.064	0.042
GRO J1008–57	3-5	0.036 (2)	0.006 (3)		10 ^g		
2S 1417–62	5-12	0.096 (3)	0.035 (6)	42.4 d	12	0.035	0.36
IGR J16320–4751	5-12	0.224 (4)	0.119 (7)	8.99 d	34	0.063	0.28
IGR J16418–4532	5-12	0.165 (5)	0.060 (9)	3.739 d	17	0.047	0.28
EXO 1722–363	5-12	0.132 (4)	0.029 (7)	9.741 d	19	0.051	0.39
IGR J18027–2016	5-12	0.189 (7)	0.03 (1)	4.569 d	16	0.069	0.37
2S 1845–024	5-12	0.069 (3)	-0.065 (7)		5 ^h		
IGR J18483–0311	5-12	0.115 (3)	-0.021 (7)	18.54 d	60	0.099	0.86
3A 1909+048 (SS 433)	5-12	0.256 (3)	0.189 (6)	13.08 d	20	0.037	0.14
4U 2206+543	1.5-12	0.376 (3)	0.252 (5)	9.558 d	17 ⁱ	0.08	0.21

^a Weighted average of the entire ASM light curve through MJD 55196 for the energy band given in column 2. A formal error based on the formal errors of the individual measurements is shown. For reference, the average intensities of the Crab Nebula are 75.503 (9), 26.825 (5), 23.290 (4), and 25.370 (5) cts s⁻¹ in the 1.5-12, 1.5-3, 3-5, and 5-12 keV bands, respectively. Note that the units of cts s⁻¹ are used as the general ASM proxy for source intensity and not for observed count rates, i.e., they give intensity in terms of the count rates due to the given source that would have been seen had SSC 1 been in the same physical condition as it was in March 1996 and had the source been in the center of its field of view.

^b Unweighted average of the entire ASM light curve through MJD 55196 for the energy band given in column 2. A formal error based on the formal errors of the individual measurements is shown. The unweighted average intensity is given for comparison with the weighted average; the difference is a rough indicator of the actual uncertainty in the average intensity.

^c Approximate peak power in the whitened and renormalized power density spectrum (see text) at the frequency given in Table 3.

^d Amplitude of a constant-amplitude sine wave that, when superposed onto the actual data, yields a peak power close to that given in column 6 (see text).

^e Ratio of the inferred average signal amplitude (A; from column 7) to the weighted average source intensity (I; from column 3).

^{f, g, h} See notes (e), (f), and (g) to Table 3.

ⁱ Power of the peak near half the frequency given in Table 3 or twice the period given in column 5.

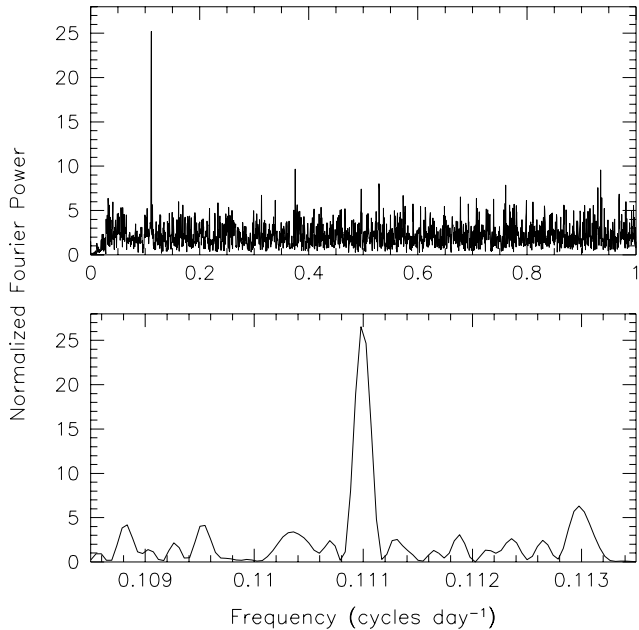


FIG. 5.— (top) Portion of a compressed power density spectrum made from the 1.5–12 keV light curve of 2S 0921–630. The “wtbx” method and a 30.0 day smoothing time scale were employed in producing the PDS. (bottom) A small region of the corresponding uncompressed PDS.

be easily detectable by other instruments.

4U 1254–69 is a so-called dipping LMXB. Its ~ 3.9 hr orbital period was revealed in both X-ray and optical observations (Courvoisier et al. 1986; Motch et al. 1987). Díaz Trigo et al. (2009) report the results of recent observations of this source with the *XMM-Newton* and *INTEGRAL* satellites. They also discuss the detection of the 3.9-hr periodicity in ASM data, present a folded light curve, and use the ASM data to obtain an estimate of the orbital period of $P = 0.16388875 \pm 0.00000017$ d ($= 3.933330 \pm 0.000004$ h). We also detect the orbital period in the ASM light curves (see Fig. 6) and derive a value for the period of $P = 3.933337 \pm 0.000010$ [± 0.000064] h (see Table 3). This value is close to that of Díaz Trigo et al. (2009) but our estimate of the uncertainty is larger. We do not believe that the ASM data alone warrant a more precise estimate of the orbital period than we have given.

4U 1323–62 is also a dipping LMXB. Parmar et al. (1989) report on *EXOSAT* X-ray observations wherein the orbital period of the binary system was manifest in terms of intensity dips that recurred with a period of $P = 2.932 \pm 0.005$ h. Later, Bałucińska-Church et al. (1999) derived a period of $P = 2.938 \pm 0.020$ h from X-ray observations with *BeppoSAX*. Even though the source is rather weak, the orbital period is easily detected in the ASM light curves (see Fig. 7). We derive a value for the period of $P = 2.941923 \pm 0.000005$ [± 0.000036] h (see Table 3). It is interesting to compare this value with the conclusion of Parmar et al. (1989) that consideration of the times of dips in two observations separated by one year imply that the period must be more precisely given by $P = 2.932128 \pm 0.000002 \pm n \times 0.000977$ h. The ambiguity in this formula reflects an ambiguity in the number of orbital cycles in the one year interval between the observations. The present determination of the orbital

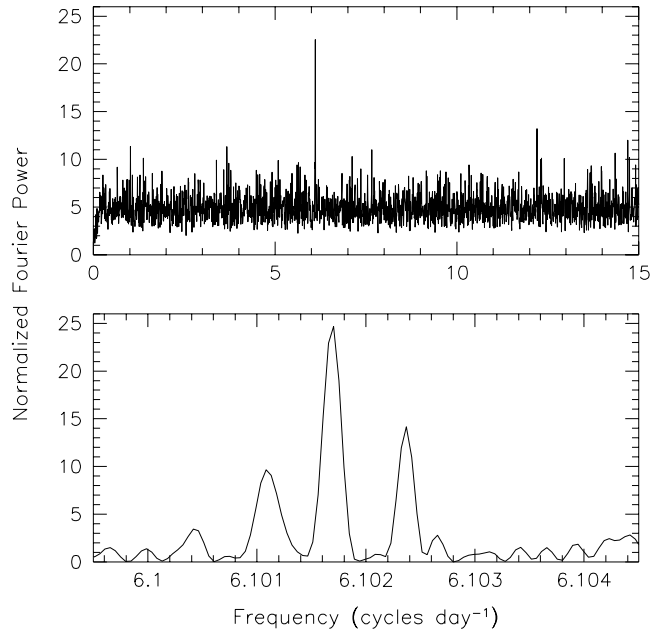


FIG. 6.— (top) Portion of a compressed power density spectrum made from the 1.5–12 keV light curve of 4U 1254–69. The “wtgs-v4” method and a 3.0 day smoothing time scale were employed in producing the PDS. (bottom) A small region of the corresponding uncompressed PDS.

period implies $n = 10$ and that $P = 2.941898 \pm 0.000005$ h where the uncertainty is dominated by the uncertainty of the correction for $n = 10$. Given that the difference between this period and the ASM-derived value is only $\Delta P = 0.000025$ h and considering the uncertainties in the two measurements, we conclude that the two values are mutually consistent. Recent studies of this source may be found in Bałucińska-Church et al. (2009) and Balman (2009).

4U 1636–536 is a persistent LMXB that often displays Type I X-ray bursts. The orbital period was found through optical photometry (Pedersen et al. 1981). It is also evident through radial velocity measurements made from emission line profiles obtained in optical spectroscopic observations (e.g., Augusteijn et al. 1998; Casares et al. 2006). Estimates of the orbital period have been successively improved by van Paradijs et al. (1990); Augusteijn et al. (1998); Giles et al. (2002) since the discovery by Pedersen et al. (1981). To our knowledge, the best optical ephemeris is that of Giles et al. (2002), who estimate that the period is $P = 3.7931263 \pm 0.0000038$ h. The ASM detection (see Figure 8) is secure, given knowledge of the optical period, but would not be sufficiently strong to have been detected in our blind search. It is, nonetheless, the first detection of the orbital period in X-rays. The period estimated from the ASM results is $P = 3.793128 \pm 0.000008$ [± 0.000060] h (Table 3). This value is consistent with that of Giles et al. (2002) though it is somewhat less precise.

4U 1728–16 (GX 9+9) is a rather bright persistent LMXB. The orbital periodicity at the period of $P = 4.19$ hours was found in *HEAO 1 A-1* X-ray data by Hertz & Wood (1988). Soon afterwards, Schaefer (1990) found variations at essentially the same period in the brightness of the optical counterpart. The ASM de-

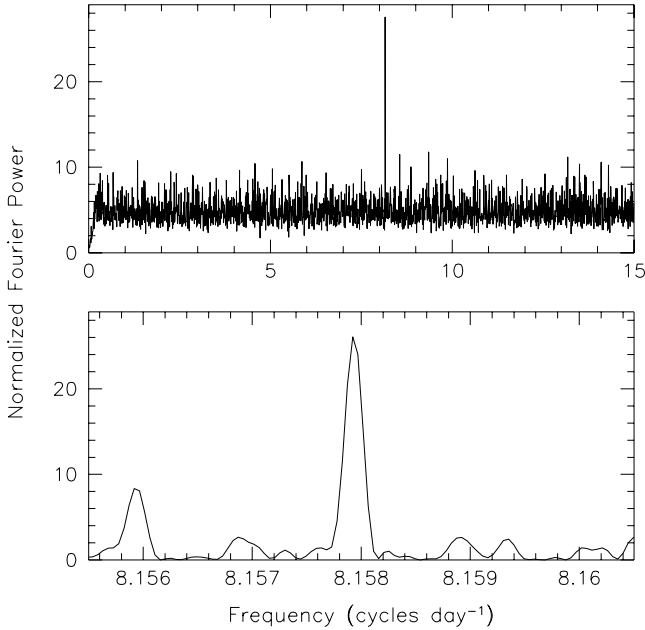


FIG. 7.— (top) Portion of a compressed power density spectrum made from the 1.5–12 keV light curve of 4U 1323–62. The “wtgs” method and a 3.0 day smoothing time scale were employed in producing the PDS. (bottom) A small region of the corresponding uncompressed PDS.

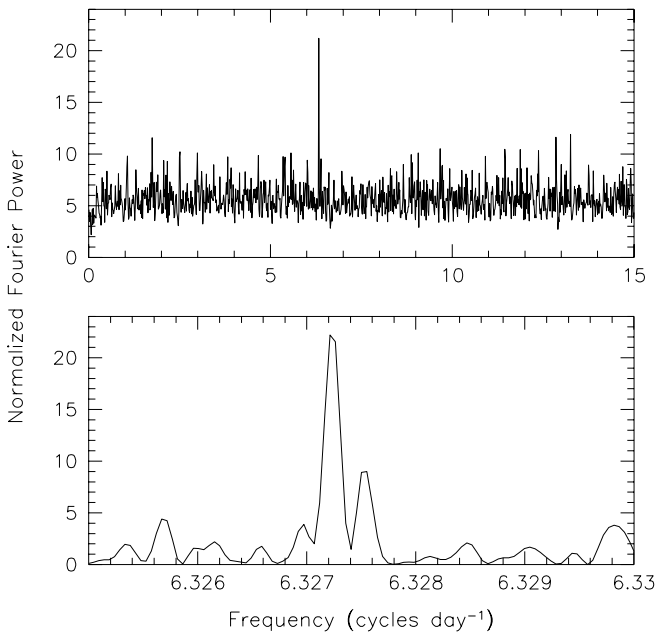


FIG. 8.— (top) Portion of a compressed power density spectrum made from the 1.5–12 keV light curve of 4U 1636–536. The “wtgs” method and a 0.9 day smoothing time scale were employed in producing the PDS. (bottom) A small region of the corresponding uncompressed PDS.

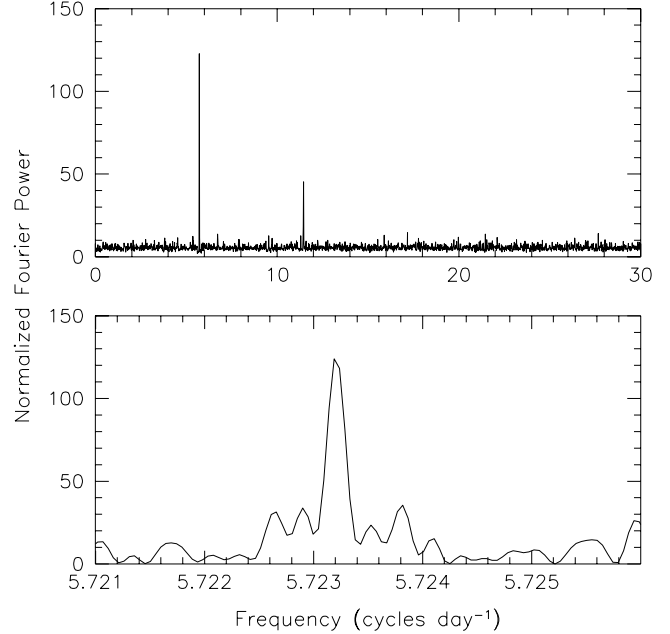


FIG. 9.— (top) Portion of a compressed power density spectrum made from the 1.5–12 keV light curve of GX 9+9. The “wtgs” method and a 0.9 day smoothing time scale were employed in producing the PDS. (bottom) A small region of the corresponding uncompressed PDS.

tection and an account of the variability in the ASM data of the modulation amplitude is described in full by Harris et al. (2009). The periodicity is manifest with even greater significance in the longer data set used in our most recent analyses; compare Fig. 9 with Fig. 2 of Harris et al. (2009). In Table 3 we also give an updated estimate of the orbital period that is only slightly different from that given by Harris et al. (2009).

4U 1746–37 is an LMXB in the globular cluster NGC 6441. X-ray observations carried out with *EXOSAT*, *Ginga*, and *RXTE/PCA* showed the presence of dips that occur roughly every 5 hours and quickly led to the interpretation that their recurrence period is the orbital period (Parmar et al. 1989; Sansom et al. 1993; Bałucińska-Church et al. 2004). The current best estimate of the orbital period, $P = 5.16 \pm 0.01$ h, was given by Bałucińska-Church et al. (2004). This periodicity is seen with high significance in the ASM data (see Fig. 10). We obtain the period estimate $P = 5.163287 \pm 0.000018 [\pm 0.000111]$ h that is consistent with the results of Bałucińska-Church et al. (2004) but is substantially more precise.

GRS 1758–258 most likely comprises a black hole accreting from a K-type giant star (Smith et al. 2002; Rothstein et al. 2002, and references therein). Smith et al. (2002) found a periodicity with $P = 18.45 \pm 0.01$ days in the data obtained in extensive *RXTE* PCA observations done in the years 1997 through 2000 and interpreted the period as the orbital period. Rothstein et al. (2002) performed near-IR observations and identified an early K-type star as the likely companion if the orbital period is as long as 18.45 days. We find a peak in the ASM power spectrum shown in Figure 11 that corresponds to a period of $P = 18.973 \pm 0.007 [\pm 0.036]$ days and that we therefore identify with

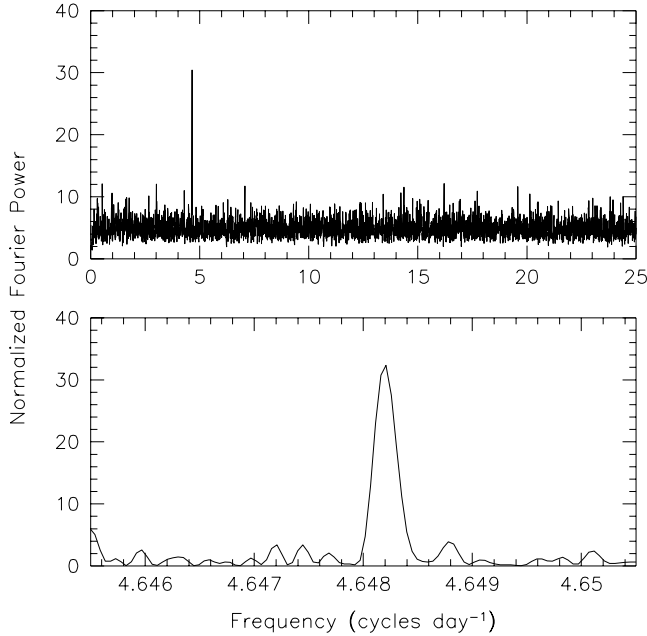


FIG. 10.— (top) Portion of a compressed power density spectrum made from the 1.5-12 keV light curve of 4U 1746–37. The “wtgs-v8” method and a 3.0 day smoothing time scale were employed in producing the PDS. (bottom) A small region of the corresponding uncompressed PDS.

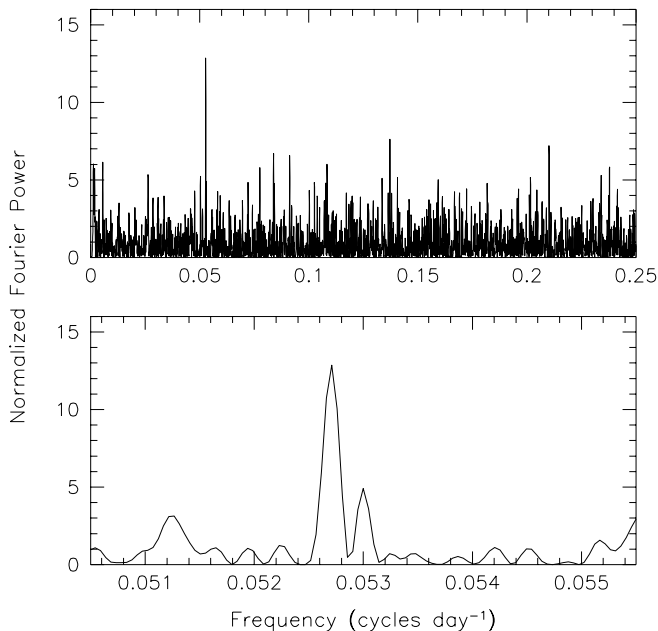


FIG. 11.— (top) Power density spectrum made from the 3-5 keV light curve of GRS 1758–258. The “wtgs” method and a 500.0 day smoothing time scale were employed in producing the PDS. (bottom) A small region of the uncompressed PDS.

the orbital period.

4U 1820–30 is a very bright LMXB in the globular cluster NGC 6624. Stella et al. (1987) analyzed data from X-ray observations with *EXOSAT* and discovered the 11 minute orbital period. The periodicity is only evident as a 3% or less peak-to-peak modulation in the

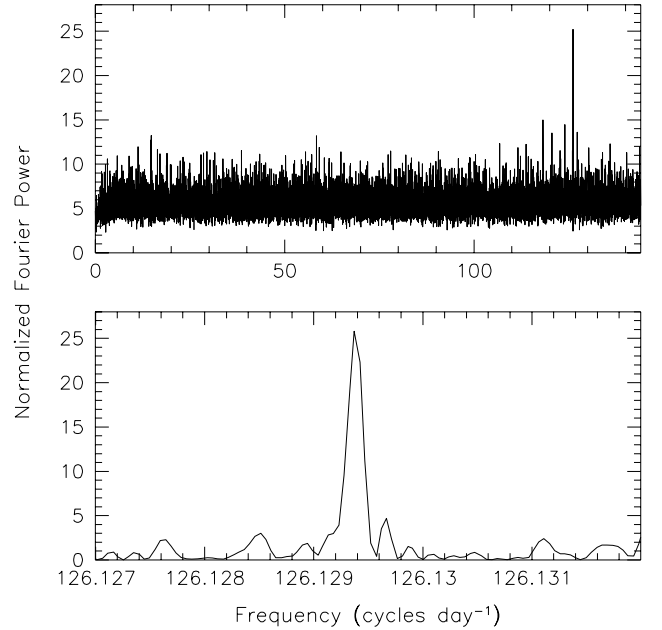


FIG. 12.— (top) Portion of a compressed power density spectrum made from the 1.5-12 keV light curve of 4U 1820–30. The “wtgs” method and a 0.9 day smoothing time scale were employed in producing the PDS. (bottom) A small region of the corresponding uncompressed PDS.

overall X-ray intensity. Chou & Grindlay (2001) used measurements made by a number of X-ray satellites of the times of maxima of the 11-m variation to obtain an ephemeris wherein both linear and quadratic terms are significant. To our knowledge, this is the most precise ephemeris in the literature at this time. We detect the periodicity in the ASM light curve with high significance; see Fig. 12 and Table 3. The period we obtain, $P = 685.01092 \pm 0.00007$ [± 0.00054] s, is an average over the duration of the ASM data set and effectively applies near the mid-time of this interval, i.e., near MJD 52620. We can compare our period measurement with the period of $P = 685.01126$ s predicted for this epoch by the Chou & Grindlay (2001) ephemeris. If we assume that the smaller of the two uncertainties in the ASM period that are given in Table 3 is applicable, then the ASM period is about 4 standard deviations below the prediction of the Chou & Grindlay (2001) ephemeris. This suggests that the coefficient of the quadratic term in that ephemeris should be more negative. However, we have not undertaken a proper joint analysis of all of the timing results and so this conclusion must be regarded as tentative.

4.2. Additional Detections of High-Mass X-ray Binaries

The orbital periods of a number of HMXBs are listed in Table 3. In contrast with the results on LMXBs, Table 3 shows that the majority of the most significant detections of these systems were made in the 5-12 keV energy band. This is in accordance with expectations based on the observation that many of the accreting compact objects in HMXBs are X-ray pulsars that tend to have relatively hard X-ray spectra.

A 0535+26 is a Be/X-ray pulsar that can be rather bright in X-rays during transient outbursts. The

early observations are reviewed by Finger et al. (1996). Pulse timing analyses of observations obtained with the BATSE instrument were used to determine that the orbital period is $P = 110.3 \pm 0.3$ days (Finger et al. 1996, and references therein). A portion of an ASM power density spectrum is shown in Figure 14. This figure demonstrates that the periodicity is apparent, but is not detected with sufficient significance to allow us to obtain a useful improvement in the precision of the orbital period. Seven separate peaks in the intensity of this source are apparent in the latter part of the ASM light curve. Their average separation is close to 114 days and is probably not consistent with the period determined through pulse timing. The outbursts of some other Be star/neutron star binaries do not occur at precisely the orbital periods determined by pulse timing, so there is no reason in this case to doubt the accuracy of the pulse timing value.

LMC X-1 is a luminous HMXB in the Large Magellanic Cloud which highly likely comprises a stellar-mass black hole and its normal OB-type companion. The properties of the system are described in detail by Orosz et al. (2009). Orosz et al. (2009) also present the ASM results and how they relate to other observations including other period determinations. Orosz et al. (2009) adopt the value of 3.90917 ± 0.00005 days as their best estimate of the period based on optical photometry and spectroscopy. An updated ASM power spectrum is shown in Figure 13 and revised estimates, based solely on the ASM power spectrum, of the orbital frequency and period are given in Table 3. We note that the ASM detection provides the only reported evidence to date of the orbital period in X-rays and that our X-ray-based period estimate of $P = 3.90898 \pm 0.00021 [\pm 0.00153]$ days is fully consistent with the optically-based value of Orosz et al. (2009).

GRO J1008–57 is a transient X-ray pulsar in a Be/X-ray binary discovered with the BATSE experiment on the *Compton Gamma-Ray Observatory* (see references in Shrader et al. 1999; Coe et al. 2007). Shrader et al. (1999) used ~ 2 years of ASM data to obtain an early estimate of the outburst period of $P \sim 135$ d. Levine & Corbet (2006) reported a relatively precise determination of the outburst period, $P_{outburst} = 248.9 \pm 0.5$ d, that was based on the time intervals between widely spaced outbursts. We believe this is still the best current estimate of the outburst cycle time. The ASM power spectrum is shown in the top panel of Figure 14. Though the peaks due to the outburst periodicity are clear, they are not sufficiently well-defined to yield a superior period estimate. Coe et al. (2007) have estimated the orbital period through timing of the 93-s pulsations seen in the BATSE data. They obtained the result $P = 247.8 \pm 0.4$ d and noted that it is in good agreement with the result of Levine & Corbet (2006).

2S 1417–62 is also a transient pulsar in a Be/X-ray binary system. A brief description of the early history and of a pulse-timing analysis using BATSE data may be found in Finger et al. (1996). The BATSE timing analysis yielded an estimate of the orbital period of $P = 42.12 \pm 0.03$ d as well as the projected semimajor axis, eccentricity, epoch of periastron passage, and other orbital elements. A slight revision to the orbital period and time of periastron passage have been given

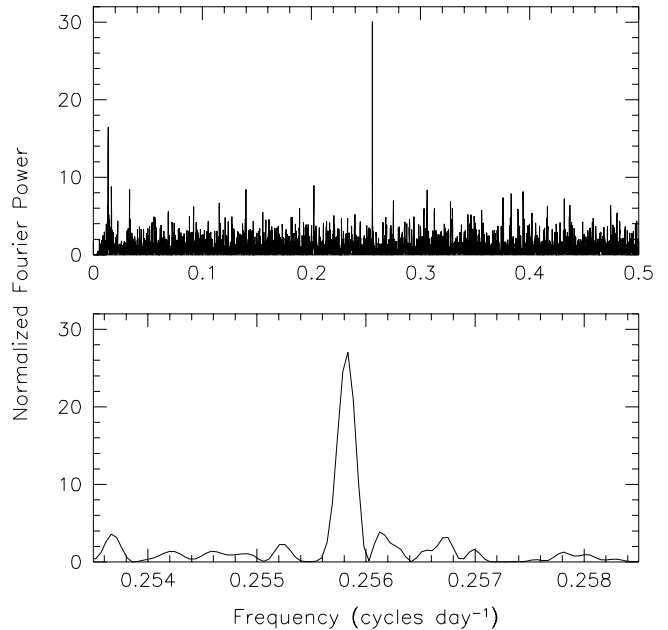


FIG. 13.— (top) Portion of a compressed power density spectrum made from the 1.5–12 keV light curve of LMC X-1. The “wtgs” method and a 100.0 day smoothing time scale were employed in producing the PDS. (bottom) A small region of the corresponding uncompressed PDS.

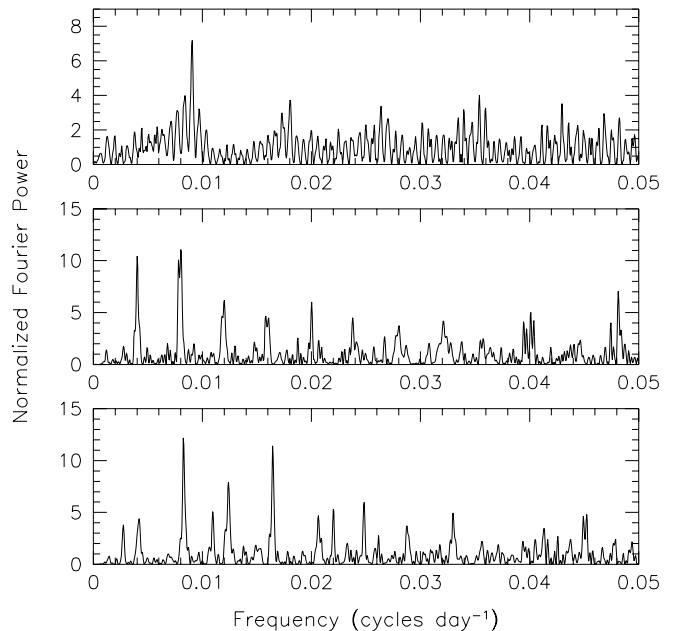


FIG. 14.— Power density spectra made using the “wtgs” method and a 500.0 day smoothing time scale. Only the low frequency regions of the power spectra are shown. (top) Power density spectrum made from the 1.5–12 keV light curve of A 0535+262. The “ringing” appearance derives from a light curve where a small number of strong outbursts punctuate the otherwise low source strength. (middle) Power density spectrum made from the 3–5 keV light curve of GRO J1008–57. (bottom) Power density spectrum made from the 5–12 keV light curve of 2S 1845–024. The previously determined orbital frequencies are 0.009066 (25) d^{-1} (A 0535+262), 0.004018 (8) d^{-1} (GRO J1008–57), and 0.0041292 (2) d^{-1} (2S 1845–024).

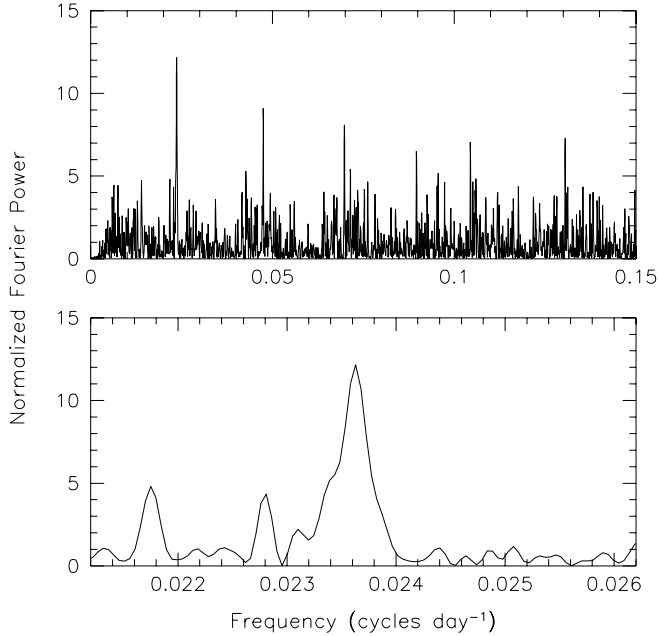


FIG. 15.— (top) Portion of a compressed power density spectrum made from the 5–12 keV light curve of 2S1417–62. The “wtgs” method and a 100.0 day smoothing time scale were employed in producing the PDS. (bottom) A small region of the corresponding uncompressed PDS. The orbital frequency determined through pulse timing is $0.02374 (2) \text{ d}^{-1}$ (see text).

by İnam et al. (2004). Evidence of outbursts recurring at intervals that are close in duration to the orbital period (or multiples thereof) is seen in the ASM power spectrum (see Fig. 15). Frequency and period estimates obtained from the spectrum shown in Fig. 15 are listed in Table 3 but are not as precise as the pulse-timing values.

IGR J16320–4751 is an X-ray pulsar with the rather long pulse period of ~ 1300 s (Lutovinov et al. 2005). Corbet et al. (2005) found the 8.96 ± 0.01 day orbital period by analyzing a *Swift* Burst Alert Telescope 14–200 keV light curve, and determined the epoch of maximum flux to be $\text{MJD } 53507.1 \pm 0.1$. Walter et al. (2006) used observations with *INTEGRAL* to measure the period, obtaining $P = 8.99 \pm 0.05$ d. The orbital period is seen at a high level of significance in the ASM power spectrum shown in Figure 16. We use the ASM power spectrum to estimate that the period is $8.9901 \pm 0.0009 [\pm 0.0081]$ d.

IGR J16418–4532 is an X-ray source in the Galactic plane that was discovered using *INTEGRAL* (Tomsick et al. 2004). Corbet et al. (2006) found and measured the orbital period using both *Swift*/BAT and ASM data and obtained the values 3.753 ± 0.004 days and 3.7389 ± 0.0004 days, respectively. Our current ASM power spectrum (Fig. 17) shows a peak that is moderately significant given prior knowledge of the period. The frequency of this peak corresponds to the period $P = 3.73886 \pm 0.00028 [\pm 0.00140]$ days. This period is essentially identical to that determined earlier from the ASM data by Corbet et al. (2006).

EXO 1722–363 is an X-ray pulsar in a high-mass binary system seen edge-on (Thompson et al. 2007, and references therein). Eclipses were found in X-ray observations made in scans of the Galactic plane with the *RXTE* PCA and their temporal spacing was used to get

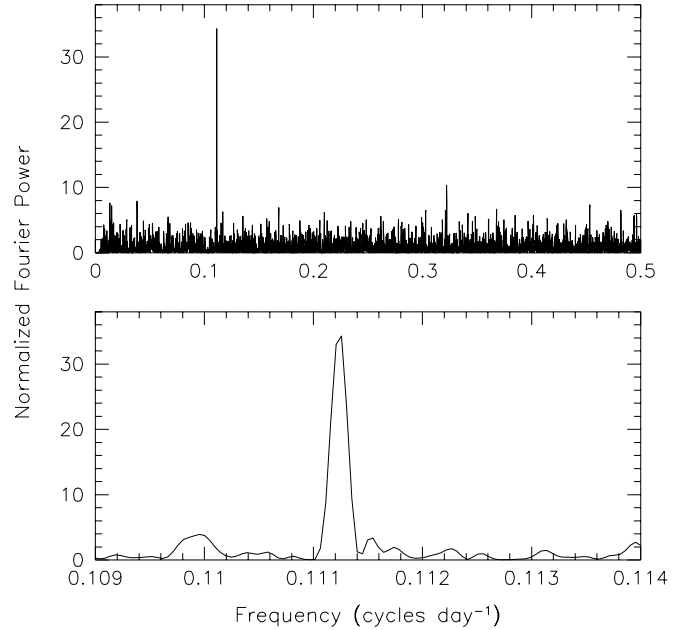


FIG. 16.— (top) Portion of a compressed power density spectrum made from the 5–12 keV light curve of IGR J16320–4751. The “wtgs” method and a 100.0 day smoothing time scale were employed in producing the PDS. (bottom) A small region of the corresponding uncompressed PDS.

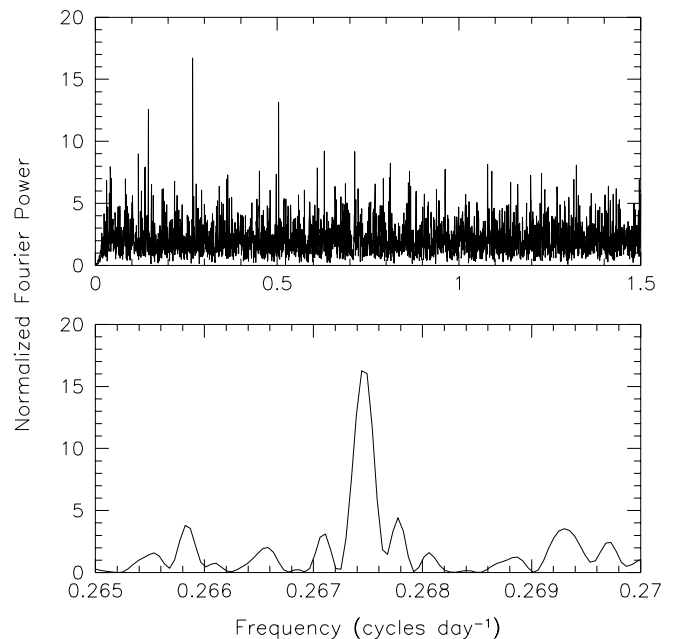


FIG. 17.— (top) Portion of a compressed power density spectrum made from the 5–12 keV light curve of IGR J16418–4532. The “wtgs” method and a 30.0 day smoothing time scale were employed in producing the PDS. (bottom) A small region of the corresponding uncompressed PDS.

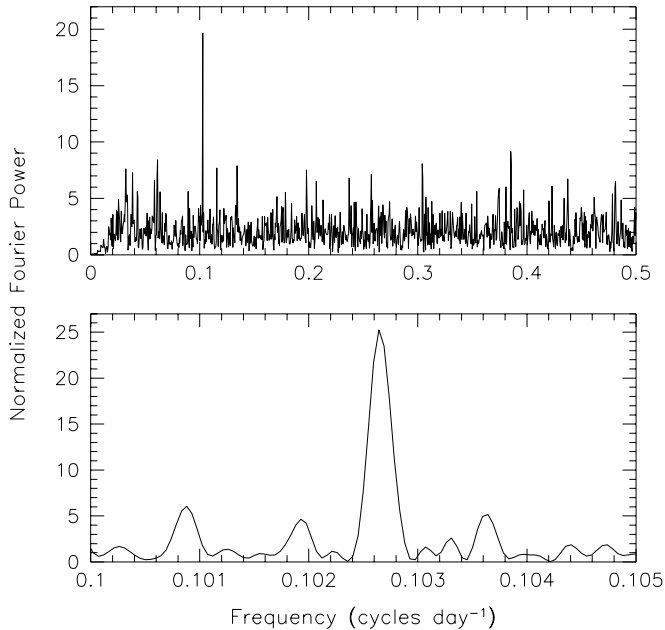


FIG. 18.— (top) Portion of a compressed power density spectrum made from the 5–12 keV light curve of EXO 1722–363. The “wtgs” method and a 30.0 day smoothing time scale were employed in producing the PDS. (bottom) A small region of the corresponding uncompressed PDS.

the first real measurement of the orbital period, i.e., $P = 9.741 \pm 0.004$ days (Corbet et al. 2005). Thompson et al. (2007) have estimated the orbital parameters through a pulse timing analysis and obtain a value for the period of $P = 9.7403 \pm 0.0004$ days. One might expect a strong signal from an eclipsing system but the source intensity is rather modest, about 4 mcrab (1.5–12 keV) on average in the ASM observations. Thus only a modest peak is evident close to the frequency in the ASM power spectrum (see Figure 18). We estimate the period to be $P = 9.7414 \pm 0.0018 [\pm 0.0095]$ days. This is consistent with but somewhat less precise than the pulse-timing-based estimate of Thompson et al. (2007). Mason et al. (2009) have recently reported estimates of the masses of the two components of the binary system and confirm that it is indeed an HMXB.

SAX J1802.7–2017 = IGR J18027–2016 is only $\sim 22'$ away from the bright X-ray source GX 9+1. It was discovered using *BeppoSAX* and, despite its proximity to a much brighter source, was found to be an X-ray pulsar in a high-mass X-ray binary system (Augello et al. 2003). Changes in the apparent pulse period led Augello et al. (2003) to infer that the pulsar is in an orbit with a period of ~ 4.6 days. Hill et al. (2005) realized that the *INTEGRAL* source IGR J18027–2016 is associated with the SAX source and refined the orbital period to be $P = 4.5696 \pm 0.0009$ days. Jain et al. (2009) used *Swift*-BAT, *INTEGRAL*-ISGRI, and *RXTE*-ASM data to estimate that the orbital period is $P = 4.5693 \pm 0.0004$ days. This periodicity is apparent in our ASM power spectra (see Fig. 19). We use the present results to estimate $P = 4.5687 \pm 0.0003 [\pm 0.0021]$ days.

2S 1845–024 = GS 1843–02 is an accreting pulsar that is evident during widely spaced outbursts (Finger et al. 1999, and references therein). A fairly pre-

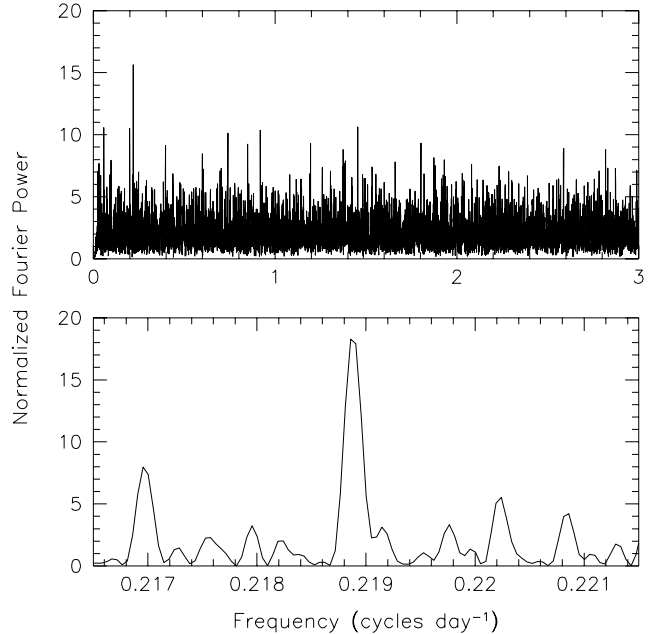


FIG. 19.— (top) Portion of a compressed power density spectrum made from the 5–12 keV light curve of IGR J18027–2016. The “wtgs” method and a 30.0 day smoothing time scale were employed in producing the PDS. (bottom) A small region of the corresponding uncompressed PDS.

cise value for the orbital period of $P = 242.18 \pm 0.01$ days was determined by Finger et al. (1999) by a pulse-timing analysis of BATSE data. A small number, ~ 5 , of outbursts are evident in the mission-long ASM light curve and the outburst periodicity is weakly evident in the ASM power spectrum (see the lower panel of Figure 14). However, the ASM results do not support a determination of an orbital period that can approach the precision of the pulse-timing-based value determined by Finger et al. (1999). Hence, we do not present an ASM-based estimate of the period.

IGR J18483–0311 was discovered in *INTEGRAL*/IBIS observations of the Galactic Center region (Chernyakova et al. 2003). The orbital period was independently found around the same time by Levine & Corbet (2006) in the ASM light curve and by Sguera et al. (2007) in the *INTEGRAL* light curve. The reported values for the period were 18.55 ± 0.03 days and 18.52 ± 0.01 days, respectively. Jain et al. (2009) have recently analyzed *Swift*/BAT and ASM data and estimate the period to be $P = 18.5482 \pm 0.0088$ days. The period is detected with high significance in the present study (see Figure 20). We use that power spectrum to estimate that the orbital period is $P = 18.545 \pm 0.003 [\pm 0.034]$ days.

3A 1909+048 is the X-ray counterpart to the well-known object **SS 433**. This object most likely consists of a stellar-mass black hole that is accreting at super-Eddington rates from a strong wind emitted by a high-mass normal-type star, and produces jets wherein the outflow velocity is approximately $0.26c$. An early review may be found in Margon (1984) and a more recent one in Fabrika (2004). The precession of the jets with a period of ~ 162 days is not only evident in the moving optical lines, but also in other phenomena including the ap-

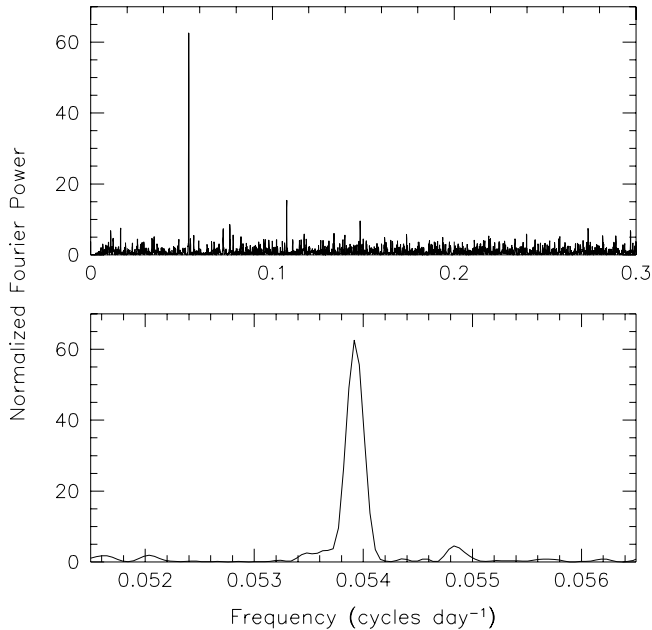


FIG. 20.— (top) Portion of a compressed power density spectrum made from the 5–12 keV light curve of IGR J18483–0311. The “wtgs” method and a 100.0 day smoothing time scale were employed in producing the PDS. (bottom) A small region of the corresponding uncompressed PDS.

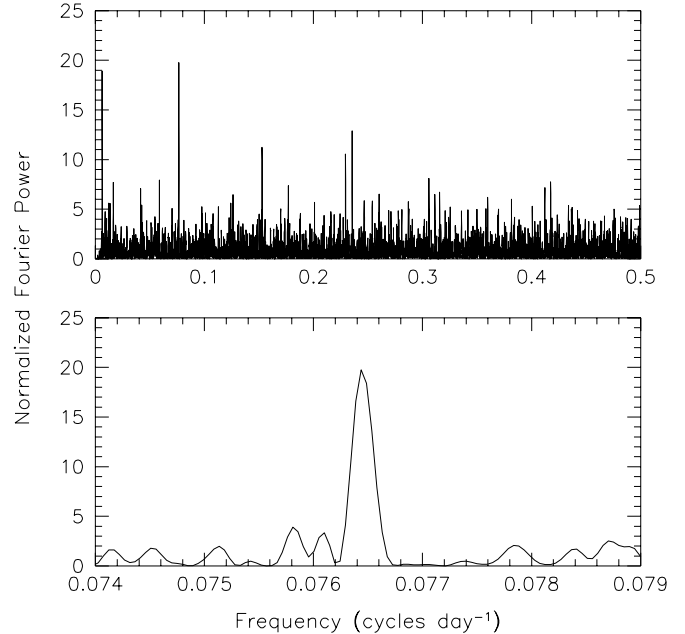


FIG. 21.— (top) Portion of a compressed power density spectrum made from the 5–12 keV light curve of SS 433. The “wtgs” method and a 100.0 day smoothing time scale were employed in producing the PDS. (bottom) A small region of the corresponding uncompressed PDS.

parent X-ray intensity (see Wen et al. 2006; Gies et al. 2002). A number of reports discuss the evidence from optical spectroscopy for Doppler shifts of the compact and normal components and their interpretation in terms of orbital parameters and component masses (see, e.g., Hillwig & Gies 2008; Cherepashchuk et al. 2009; Kubota et al. 2010). Goranskii et al. (1998) reported a precise measurement of the orbital period of the binary, i.e., $P_{orb} = 13.08211 \pm 0.00008$ days, on the basis of the times of eclipse-like dips in the optical flux. The X-ray intensity also shows eclipse-like dips (e.g., Filippova et al. 2006; Cherepashchuk et al. 2009) but these have not yet been exploited for orbital period estimation. Gies et al. (2002) reported the first evidence of the orbital period in the ASM X-ray intensity measurements. Very recently, Kubota et al. (2010) obtained a new time of minimum optical brightness and used it, together with the earlier observations, to obtain a revised value of the period, $P_{orb} = 13.08227 \pm 0.00008$ d. In the present analysis, we find unambiguous evidence of both the precession and the orbital periods in the power spectrum (see Figure 21). Our estimate of the orbital period is $P_{orb} = 13.080 \pm 0.003$ [± 0.017] days. This value is consistent with, but somewhat less precise than, those of Goranskii et al. (1998) and Kubota et al. (2010). If we fold the ASM light curve with the period and epoch of Kubota et al. (2010), we find that the time of X-ray minimum is coincident with the time of optical minimum. The shape of the folded ASM light curve is similar to the eclipse-like shapes seen by *INTEGRAL* (e.g., Cherepashchuk et al. 2009) and suggests that the eclipse-like decrease in the flux is the result of periodically occurring partial occultations of the X-ray emitting regions, broadly construed to include regions where the X-ray flux

may be scattered (see Fig. 4).

4U 2206+543 is a high-mass X-ray binary which manifests a distinct variation at a period of $P \approx 9.6$ days in the ASM light curve (Corbet & Peele 2001). This source is included in this report even though the ~ 9.6 -day period was reported by Wen et al. (2006) because the underlying period may actually be twice as long, or ~ 19.2 days (Corbet et al. 2007b; see also Wang 2009). In this regard, Corbet et al. (2007b) found a signal at a period of $P = 19.25 \pm 0.08$ days in *Swift*/BAT data and a signal near the same period in ASM data. Wang (2009) found a peak near a period $P = 19.11$ days in the ASM data. Our power spectrum of ASM data also shows peaks at frequencies corresponding to both periods (see Figure 22). The more significant peak corresponds to a period of $P = 9.5584 \pm 0.0012$ [± 0.0091] days. Assuming that the subharmonic corresponds to a period twice this value, we obtain $P = 19.117 \pm 0.003$ [± 0.018] days. Radial velocity measurements from optical or near IR spectroscopy are needed to unambiguously determine the true orbital period.

4.3. Nondetections and Search Sensitivity

The estimates of the amplitudes of the periodic signals that are reported in Table 4 fall, for most of the cases, just below the detection thresholds of the present blind search. They thereby illustrate the typical sensitivity of the present search. We have also estimated the amplitudes that approximately correspond to our detection thresholds in a set of additional sources chosen either to help cover a wide range of intensities or because they are of interest for other reasons. To accomplish this we have computationally superimposed sine waves onto the ASM light curves and repeated the search analyses on the light curves for those particular sources in order to

TABLE 5
UPPER LIMITS ON SELECTED PERIODICITIES

Source Name	Band (keV)	Intensity ^a (cts s ⁻¹)	Period ^b	Filter Time ^c (days)	Amplitude ^d (cts s ⁻¹)	A/I ^e
Crab Nebula	1.5-12	75.50 (1)		3.0	0.12	0.0016
Sco X-1	1.5-12	867.81 (6)	0.789 d	3.0	7.2	0.0082
Sco X-1	1.5-12	867.81 (6)	0.789 d	10.0	8.5	0.0099
GX 340+0	1.5-12	28.657 (8)		3.0	0.36	0.013
GRO J1655-40	1.5-12	5.311 (7)	2.62 d	30.0	0.30	0.056
GX 339-4	1.5-12	4.337 (6)	1.75 d	10.0	0.083	0.019
4U 1735-444	1.5-12	12.739 (7)	4.65 h	3.0	0.11	0.0089
GX 5-1	1.5-12	69.30 (1)		3.0	0.75	0.011
V4641 Sgr	1.5-12	0.458 (9)	2.80 d	30.0	0.13	0.28
4U 1957+115	1.5-12	2.366 (4)	9.33 h	3.0	0.040	0.017

^a Weighted average of the entire ASM light curve. See note (a) to Table 4.

^b Approximate orbital period if reported. See the following references for previous period determinations and more precise values: Vanderlinde et al. 2003 (Sco X-1); Greene et al. 2001 (GRO J1655-40); Hynes et al. 2003 (GX339-4); Casares et al. 2006 (4U 1735-444); Orosz et al. 2001 (V4641 Sgr); Thorstensen 1987 (4U 1957+115);

^c See text and column 1 of Table 2.

^d Amplitude which would have been likely to yield a peak of ~ 25 in the power density spectrum.

^e Ratio of the signal amplitude that would yield a peak power of 25 (A; from column 6) to the average source intensity (I; from column 3).

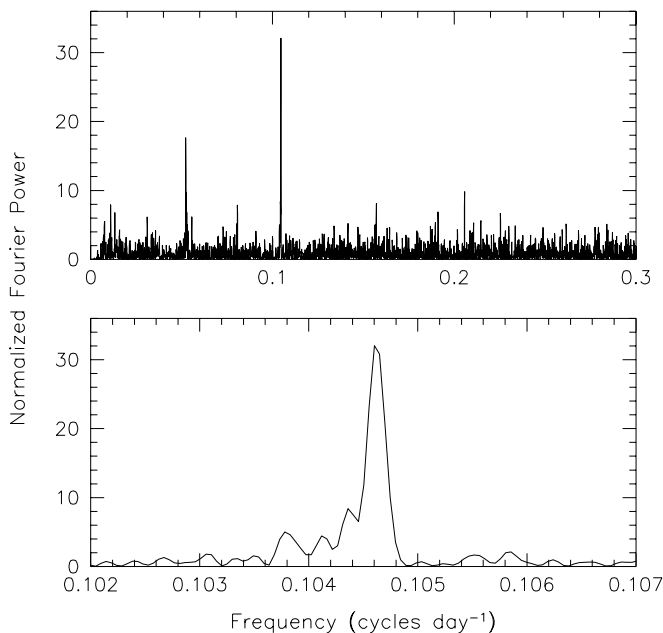


FIG. 22.— (top) Portion of a compressed power density spectrum made from the 1.5-12 keV light curve of 4U 2206+543. The “wtbx” method and a 100.0 day smoothing time scale were employed in producing the PDS. (bottom) A small region of the corresponding uncompressed PDS.

determine the signal amplitudes that would have resulted in peaks reaching renormalized whitened powers of ~ 25 in the power density spectra. These estimates, which may be taken as upper limits since we would have recognized peaks near these frequencies that reached powers as small as 15, are listed in Table 5. This table also lists previously reported periods for some of the sources as well as mission-average intensities. Column 7 of the table gives the effective upper limits on the amplitudes as fractions of the average source intensities.

Levine & Corbet (2006) reported modest significance detections of periodicities in ASM power density spectra for GRO J1655-40, GX 339-4, V4641 Sgr, and 4U 1957+115 at or very close to the periods previously reported in the literature. In the analyses using the entire ASM light curves that we have done recently we do not confirm these possible detections. Results of sensitivity analyses for these sources are included in Table 5.

Table 5 also includes entries for two bright sources, Sco X-1 and 4U 1735-444, with well-established periodicities that we do not detect as well as entries for three sources, i.e., the Crab Nebula, GX 340+0, and GX 5-1, that do not have known orbital periodicities. Table 5 gives upper limits, calculated as described above, on any modulation near the reported periods. We note that for Sco X-1 the noise is dominated by the intrinsic source variations. In rare cases, such as that described by Vanderlinde et al. (2003), specialized techniques may be available to partially mitigate the effects of the intrinsic variation and improve the sensitivity of a periodicity search. We have not tried to apply any such techniques in the present general search. The upper limits on periodicities in the power spectra for the Crab, GX 340+0, and GX 5-1 are included in this table to illustrate the typical sensitivity of the present search in the cases of bright sources.

We also did not detect the alias of the 290-s pulse period in X1145-619 that was reported in Levine & Corbet (2006). This is not so unexpected since pulse periods tend to change more rapidly than orbital periods and could change to a degree that makes them significantly noncoherent and therefore hard to detect in a 14-yr data set.

In short, Tables 4 and 5 show that the search sensitivity depends on a number of factors including source strength, degree of intrinsic source variability, and quality of the ASM light curve (which, in turn depends on the source location relative to nearby bright sources, etc.).

The present search for periodicities in the ASM light curves has proved to be more sensitive than the earlier search done by Wen et al. (2006). The weighting and filtering aspects of our search algorithms have proved to be major factors in the sensitivity improvements. Another major factor is the use of light curves that cover ~ 5 more years. The result is the detection of the orbital periods in 8 LMXBs and in ~ 12 HMXBs that were not detected by Wen et al. (2006). Our detection of the 18.55-d period of IGR J18483–0311 represents the co-discovery with Sguera et al. (2007) of the orbital period of this system. Our detections of the orbital periods of 4U 1636–536 and LMC X-1 are the first for these systems, to our knowledge, that have been accomplished on the basis of X-ray observations.

It is interesting to compare the present list of detections together with those of Wen et al. (2006) with Tables 1.1 and 1.3 of White et al. (1995) that list the well-established orbital periods of LMXBs and HMXBs as of 1994 or 1995. Table 1.1 of White et al. (1995) lists 32 LMXBs with known orbital periods. Of these, seven have been in quiescence through the entire RXTE mission and one (CAL 87) is a supersoft source that emits at energies below the ASM band; these systems would not be expected to yield periodicity detections in ASM data. The periodicities of 17 of the remaining 24 systems have now been detected in the ASM light curves if we include Sco X-1 per the results of Vanderlinde et al. (2003) even though its orbital period was not detected in the present study. Seven systems that are detected by the ASM by virtue of their intensities do not yield period detections in the present search. The ASM periodicity searches have yielded clear detections of the orbital periods of 13 of the 16 systems listed in Table 1.1 of White et al. (1995) that had, at that time, shown evidence of the orbital period in X-rays (see column 5 therein). Two of the remaining three systems have been in quiescence throughout the RXTE mission. The last remaining system is Cyg X-2 for which we find no evidence of the 9.8-d period even though it is rather bright in X-rays.

Table 1.3 of White et al. (1995) lists 24 HMXBs with known orbital periods. Of these, only one (X0535–668)

has been in quiescence during the entire RXTE mission. The orbital periodicities of 16 of the remaining 23 systems have been clearly detected in power density spectra of the ASM light curves; we do not count X0535+262 as a clear detection in the power spectrum. The periods of four of the systems (X0115+634, X0535+262, GX 304–1, and X1145–619) are apparent in the ASM light curves as limited sequences of short transient outbursts that are separated by the orbital period or small multiples thereof. The HMXBs X1553-542 and X0331+530 are evident in the ASM light curves during short transient outbursts, but the ASM yields no evidence of their orbital periods. We also find no evidence of the 1.7-d period of LMC X-3 even though it is detectable over most of the 14-year time of the RXTE mission.

Not unexpectedly, we find that the amplitudes of the variations at the orbital period, when expressed as fractions of the average intensity, are typically low for LMXBs and high for HMXBs (see Tables 4 and 5). This is consistent with the relatively low rate of detections of orbital modulation in LMXBs and the high rate in HMXBs. There are some exceptions such as the high fractional modulation of the weak LMXB 2S 0921–630 and the low degree of modulation of the HMXBs LMC X-1 and LMC X-3. Our results for 2S 0921–630 suggest that there could be other weak LMXBs with fractional amplitudes that are not particularly low and that would not be difficult to detect with an instrument somewhat more sensitive than the ASM. Indeed, it is likely that the MAXI instrument on the International Space Station (Matsuoka et al. 2009) will produce light curves useful for extending the search for periodicities in X-ray light curves and will be able to find many additional periodicities and orbital periods.

We gratefully acknowledge the efforts of the RXTE/ASM science teams at MIT and NASA/GSFC, and the RXTE mission support groups at GSFC. We thank Alex Camacho for computing the upper limits presented in Table 5. We acknowledge the support of NASA through Contract NAS 5-30612 (MIT).

REFERENCES

- Augello, G., Iaria, R., Robba, N. R., Di Salvo, T., Burderi, L., Lavagetto, G., & Stella, L. 2003, *ApJ*, 596, L63
- Augustejn, T., van der Hooft, F., de Jong, J. A., van Kerkwijk, M. H., & van Paradijs, J. 1998, *A&A*, 332, 561
- Balman, S. 2009, *AJ*, 138, 50
- Balućńska-Church, M., Church, M. J., Oosterbroek, T., Segreto, A., Morley, R., & Parmar, A. N. 1999, *A&A*, 349, 495
- Balućńska-Church, M., Church, M. J., & Smale, A. P. 2004, *MNRAS*, 347, 334
- Balućńska-Church, M., Dotani, T., Hirotsu, T., & Church, M. J. 2009, *A&A*, 500, 873
- Bodaghee, A., et al. 2007, *A&A*, 467, 585
- Branduardi-Raymont, G., Corbet, R., Parmar, A. N., Murdin, P. G., & Mason, K. O. 1981, *Space Science Reviews*, 30, 279
- Casares, J., Cornélisse, R., Steeghs, D., Charles, P. A., Hynes, R. I., O’Brien, K., & Strohmayer, T. E. 2006, *MNRAS*, 373, 1235
- Cherepashchuk, A. M., Sunyaev, R. A., Postnov, K. A., Antokhina, E. A., & Molkov, S. V. 2009, *MNRAS*, 397, 479
- Chernyakova, M., Lutovinov, A., Capitanio, F., Lund, N., & Gehrels, N. 2003, *The Astronomer’s Telegram*, 157, 1
- Chevalier, C., & Ilovaisky, S. A. 1981, *A&A*, 94, L3
- Chou, Y., & Grindlay, J. E. 2001, *ApJ*, 563, 934
- Coe, M. J., et al. 2007, *MNRAS*, 378, 1427
- Corbet, R., et al. 2005, *The Astronomer’s Telegram*, 649, 1
- Corbet, R., et al. 2006, *The Astronomer’s Telegram*, 779, 1
- Corbet, R., et al. 2007, *Progress of Theoretical Physics Supplement*, 169, 200 (arXiv:astro-ph/0703274)
- Corbet, R. H. D., Markwardt, C. B., & Swank, J. H. 2005, *ApJ*, 633, 377
- Corbet, R. H. D., Markwardt, C. B., & Tueller, J. 2007, *ApJ*, 655, 458
- Corbet, R. H. D., & Peele, A. G. 2001, *ApJ*, 562, 936
- Courvoisier, T. J.-L., Parmar, A. N., & Peacock, T. 1985, *Space Science Reviews*, 40, 275
- Courvoisier, T. J.-L., Parmar, A. N., Peacock, A., & Pakull, M. 1986, *ApJ*, 309, 265
- Díaz Trigo, M., Parmar, A. N., Boirin, L., Motch, C., Talavera, A., & Balman, S. 2009, *A&A*, 493, 145
- Fabrika, S. 2004, *Astrophysics and Space Physics Reviews*, 12, 1
- Filippova, E., Revnivtsev, M., Fabrika, S., Postnov, K., & Seifina, E. 2006, *A&A*, 460, 125
- Finger, M. H., Bildsten, L., Chakrabarty, D., Prince, T. A., Scott, D. M., Wilson, C. A., Wilson, R. B., & Zhang, S. N. 1999, *ApJ*, 517, 449

- Finger, M. H., Wilson, R. B., & Chakrabarty, D. 1996, *A&AS*, 120, 209
- Finger, M. H., Wilson, R. B., & Harmon, B. A. 1996, *ApJ*, 459, 288
- Gies, D. R., McSwain, M. V., Riddle, R. L., Wang, Z., Wiita, P. J., & Wingert, D. W. 2002, *ApJ*, 566, 1069
- Giles, A. B., Hill, K. M., Strohmayer, T. E., & Cummings, N. 2002, *ApJ*, 568, 279
- Goranskii, V. P., Esipov, V. F., & Cherepashchuk, A. M. 1998, *Astronomy Reports*, 42, 209
- Greene, J., Bailyn, C. D., & Orosz, J. A. 2001, *ApJ*, 554, 1290
- Harris, R. J., Levine, A. M., Durant, M., Kong, A. K. H., Charles, P., & Shahbaz, T. 2009, *ApJ*, 696, 1987
- Hertz, P., & Wood, K. S. 1988, *ApJ*, 331, 764
- Hill, A. B., et al. 2005, *A&A*, 439, 255
- Hillwig, T. C., & Gies, D. R. 2008, *ApJ*, 676, L37
- Horne, J. H., & Baliunas, S. L. 1986, *ApJ*, 302, 757
- Hynes, R. I., Steeghs, D., Casares, J., Charles, P. A., & O'Brien, K. 2003, *ApJ*, 583, L95
- İnam, S. Ç., Baykal, A., Matthew Scott, D., Finger, M., & Swank, J. 2004, *MNRAS*, 349, 173
- Jain, C., Paul, B., & Dutta, A. 2009, *Research in Astronomy and Astrophysics*, 9, 1303
- Jonker, P. G., Steeghs, D., Nelemans, G., & van der Klis, M. 2005, *MNRAS*, 356, 621
- Kubota, K., Ueda, Y., Fabrika, S., Medvedev, A., Barsukova, E. A., Sholukhova, O., & Goranskij, V. P. 2010, *ApJ*, 709, 1374
- Levine, A. M., Bradt, H., Cui, W., Jernigan, J. G., Morgan, E. H., Remillard, R., Shirey, R. E., & Smith, D. A. 1996, *ApJ*, 469, L33
- Levine, A. M., & Corbet, R. 2006, *The Astronomer's Telegram*, 940, 1
- Liu, Q. Z., van Paradijs, J., & van den Heuvel, E. P. J. 2006, *A&A*, 455, 1165
- Liu, Q. Z., van Paradijs, J., & van den Heuvel, E. P. J. 2007, *A&A*, 469, 807
- Lutovinov, A., Rodriguez, J., Revnivtsev, M., & Shtykovskiy, P. 2005, *A&A*, 433, L41
- Margon, B. 1984, *ARA&A*, 22, 507
- Mason, A. B., Norton, A. J., Clark, J. S., Negueruela, I., & Roche, P. 2009, arXiv:0911.4887
- Mason, K. O., Branduardi-Raymont, G., Codova, F. A., & Corbet, R. H. D. 1987, *MNRAS*, 226, 423
- Matsuoka, M., et al. 2009, *PASJ*, 61, 999
- Motch, C., Pedersen, H., Courvoisier, T. J.-L., Beuermann, K., & Pakull, M. W. 1987, *ApJ*, 313, 792
- Orosz, J. A., et al. 2001, *ApJ*, 555, 489
- Orosz, J. A., et al. 2009, *ApJ*, 697, 573
- Parmar, A. N., Gottwald, M., van der Klis, M., & van Paradijs, J. 1989, *ApJ*, 338, 1024
- Parmar, A. N., Stella, L., & Giommi, P. 1989, *A&A*, 222, 96
- Pedersen, H., van Paradijs, J., & Lewin, W. H. G. 1981, *Nature*, 294, 725
- Press, W. H., Teukolsky, S. A., Vetterling, W. T., & Flannery, B. P. 1992, "Numerical recipes in C. The art of scientific computing", 2nd ed., Cambridge: Cambridge University Press
- Reig, P., Torrejón, J. M., Negueruela, I., Blay, P., Ribó, M., & Wilms, J. 2009, *A&A*, 494, 1073
- Ribó, M., Negueruela, I., Blay, P., Torrejón, J. M., & Reig, P. 2006, *A&A*, 449, 687
- Rothstein, D. M., Eikenberry, S. S., Chatterjee, S., Egami, E., Djorgovski, S. G., & Heindl, W. A. 2002, *ApJ*, 580, L61
- Sansom, A. E., Dotani, T., Asai, K., & Lehto, H. J. 1993, *MNRAS*, 262, 429
- Scargle, J. D. 1982, *ApJ*, 263, 835
- Schaefer, B. E. 1990, *ApJ*, 354, 720
- Sguera, V., et al. 2007, *A&A*, 467, 249
- Shahbaz, T., Casares, J., Watson, C. A., Charles, P. A., Hynes, R. I., Shih, S. C., & Steeghs, D. 2004, *ApJ*, 616, L123
- Shahbaz, T., & Watson, C. A. 2007, *A&A*, 474, 969
- Shrader, C. R., Sutaria, F. K., Singh, K. P., & Macomb, D. J. 1999, *ApJ*, 512, 920
- Smith, D. M., Heindl, W. A., & Swank, J. H. 2002, *ApJ*, 578, L129
- Steeghs, D., & Jonker, P. G. 2007, *ApJ*, 669, L85
- Stella, L., Friedhorsky, W., & White, N. E. 1987, *ApJ*, 312, L17
- Thompson, T. W. J., Tomsick, J. A., in 't Zand, J. J. M., Rothschild, R. E., & Walter, R. 2007, *ApJ*, 661, 447
- Thorstensen, J. R. 1987, *ApJ*, 312, 739
- Tomsick, J. A., Lingelfelter, R., Corbel, S., Goldwurm, A., & Kaaret, P. 2004, *The Astronomer's Telegram*, 224, 1
- Vanderlinde, K. W., Levine, A. M., & Rappaport, S. A. 2003, *PASP*, 115, 739
- van Paradijs, J., et al. 1990, *A&A*, 234, 181
- Walter, R., et al. 2006, *A&A*, 453, 133
- Wang, W. 2009, *MNRAS*, 398, 1428
- Wen, L., Levine, A. M., Corbet, R. H. D., & Bradt, H. V. 2006, *ApJS*, 163, 372
- White, N. E., Nagase, F., & Parmar, A. N. 1995, in *X-ray binaries*, eds. W. H. G. Lewin, J. van Paradijs, & E. P. J. van den Heuvel, 1